# Multiparameter monitoring of crevasses on an Alpine glacier to understand formation and evolution of snow bridges

L. Ravanel, E. Lacroix, E. Le Meur, P. Batoux, E. Malet

# Multiparameter monitoring of crevasses on an Alpine glacier to understand formation and evolution of snow bridges

L. Ravanel[a,b*], E. Lacroix[a], E. Le Meur[d], P. Batoux[c], E. Malet[a]

[a] EDYTEM, Univ. Savoie Mont-Blanc, CNRS (UMR 5204), 73370 Le Bourget du Lac, France

[b] Department of Geosciences, University of Oslo, Sem Sælands vei 1, 0371 Oslo, Norway

[c] ENSA, ENSM, 74400 Chamonix, France

[d] IGE, Univ. Grenoble Alpes, CNRS, IRD, Grenoble INP, 38000 Grenoble, France

[*] Corresponding author at: EDYTEM, Univ. Savoie Mont-Blanc, CNRS (UMR 5204), 73370 Le Bourget du Lac, France

E-mail address: Ludovic.Ravanel@univ-smb.fr (L. Ravanel).

**Abstract**

On glaciers, the snow bridges that form above crevasses have hardly been considered by researchers up to now, despite their importance for high mountain activities (skiing, mountaineering) and the risks that their possible failure poses to practitioners. In order to improve our understanding of the formation and evolution of these fragile snow structures, we monitored during two years a succession of three crevasses located at 3450 m a.s.l. in the Mont-Blanc massif (France) using a set of sensors including an automatic camera, air temperature sensors, a wind vane-anemometer, and an extensometer. Geophysical profiles (ground penetrating RaDAR) were also carried out to clarify the glacial context. Despite particularly extreme monitoring conditions, at the level of a bump formed by the bedrock under an ice thickness of *c*. 25 m, we have shown that a wind event parallel to the crevasse favours its filling by snow while a strong wind making a significant angle with the crevasse under largely negative temperatures can rapidly create a snow bridge by cornice accretion that grows by extending

leeward. High temperatures are responsible for most of the natural failures of SBs. These elements are already used for risk mitigation.

**Keywords:** Glaciers, Crevasses, Snow bridges, Snow transport, Cornice accretion, Mechanical failure, Mont Blanc massif.

## 1. Introduction

Crevasses are a major concern for people who move on glaciers because of the risk to life they pose. Falls are most frequently associated with the failure of snow bridges (SBs) which can form above crevasses more or less durably, mostly under the form of an arch thereby making it difficult to detect the underneath crevasses. While a SB can generally support its own weight, this is sometimes no longer true when overload (skier, mountaineer). SBs strength is difficult to assess and these snow structures have so far been the subject of almost no study.

Crevasses are fractures that form in response to tensile strain in glaciers (Hopkins, 1892; Smith, 1976; Vaughan, 1993; van der Veen, 1998, 1999). Crevasses initiate at or near the surface of the ice, generally from starter microcracks (Pralong and Funk, 2005) that propagate downward into the ice as long as the tensile strain remains sufficient, until the weight-induced lithostatic strength prevents them from penetrating any deeper (Holdsworth, 1969; Nath and Vaughan, 2003). Most of the time, crevasses are aligned perpendicular to the direction of the main tensile strain (Vaughan, 1993; van der Veen, 1999). Crevasse patterns usually reflect either high- or low-advection lifecycles (Colgan et al., 2016). High-advection lifecycle refers to crevasses that are opening in the upper part of glaciers due to local stress fields (*e.g.*, acceleration in ice velocity) and closing in downstream locations (deceleration). Crevasse patterns are more transient in low-advection lifecycles, with crevasses constantly opening/closing with limited horizontal advection. High-advection lifecycles are more likely for transverse crevasses in the

glacier accumulation zone (Hambrey and Müller, 1978; Vornberger and Whillans, 1990), while low-advection lifecycles are more likely for crevasses in the glacier ablation zone (Harper et al., 1998). In the Alps, field experiences indicate that crevasses can be several tens/hundreds of meters long. Their depth can range from a few meters to 20-30 m, while their width rarely exceeds 6 to 8 m. These dimensions explain the potentially fatal nature of falls in crevasses for mountaineers and skiers, especially when the whole SB collapses (Fig. 1).

Data related to crevasses accidents are rather sparse and scattered but these accidents most of the time involve the failure of a SB. On the French side of the Mont-Blanc massif (MBM; Western European Alps), the French *National Mountain Safety Observation System* (SNOSM) recorded 170 climbers who died during the summers 2003 to 2012, 6 of which (3 %) from a fall into a crevasse. Over the period 2008-2014, in the same area but outside the *Vallée Blanche* ski itinerary (which is however the most famous and frequented off-piste ski route), there were 37 injuries and 13 deaths (2 per year in average) due to falls into crevasses. Between Oct. 2015 and July 2021 (nearly 6 years), 63 people have been rescued for such an accident as part of the practice of mountaineering (excluding skiing) in the French Alps (data: SNOSM). Among them, 32 were reported safe (51 %), 26 were injured (41 %) and 5 faced traumatic deaths (8 %). Being both the most glacierized (Gardent et al., 2014) and frequented (Salim et al., 2019), the MBM is predominantly represented (86 % of people rescued). The accidents occurred at an average altitude of 3160 m a.s.l., *i.e.* around the current regional glacier equilibrium line altitude (Rabatel et al., 2013), most often in the middle of the day (*c*. 01:30 p.m.), in summer (68 % between July and Aug.) – which also corresponds to the period of highest activity –, and during sunny and hot weather conditions (70 %). Sometimes, accidents involve the failure of large SBs as a whole. Pasquier et al. (2014) and Klocker et al. (2022) retrospectively reviewed helicopter-based emergency services rescue missions for crevasse victims in Switzerland over the periods 2000-2010 (415 victims) and 2010-2020 (321 victims), respectively, with a clinical spectrum of injuries ranging from benign to lethal. During the first period, the mean depth of fall was 16.5 m and death occurred for 11 % of the victims. Overall on-site mortality was higher during the ski season compared to the rest of the year (*i.e.* mainly

summer) with higher mean depth of fall (22 *vs*. 15 m). During the second period, the overall mortality was 6.5 %. The mean depth of fall was 15 m during the winter season compared to 8 m during the summer. For both periods, injury severity positively correlates with the depth of fall.

A better understanding of the often temporary and fragile structures that constitute the SBs is thus necessary to improve prevention so as to reduce accidents (*e.g.*, Mourey et al., 2019).

There was no study on SBs outside that of Rochelle and Rochelle (2006) who calculated the forces involved in a modelled isotropic SBs and discussed the effects of different modes of movement on top (walking, snowshoeing, skiing). The revealed potential types of failure are: (i) footprint-induced shear (perforating failure), (ii) shear at the edges of SBs, and (iii) flexure (tensile failure). Shortest falls correspond to type 1 and longest falls to type 3. Facing the on-going lack of knowledge, Ogier et al. (2017) designed and disseminated two online questionnaires to gain knowledge based on experience: one on incidents/accidents, the other on the management of the specific risk of SB failure. They were intended to skiers and mountaineers who had already been confronted to such a failure in the Western Alps, either as a victim or as a witness. There were 209 and 297 usable responses, respectively. Once again, the accidents mainly occurred between 3000 and 3500 m a.s.l.; 20 cases reported a failure of a SB whose thickness was greater than 1.5 m with wet or powder snow on the surface. The total collapse of the SB (see for instance Fig. 1) concerned 24 cases (12 %) and often led to serious traumatic consequences. The middle of the SB, where its thickness was generally the lowest, often appeared to be the weakness point: failure at this location represented 70 % of the reported cases. The authors also confirm the modalities of failure proposed by Rochelle and Rochelle (2006).

To improve crevasse risk management and to have a better understanding of this natural object, observational data are needed, especially to understand how SBs are formed, how they evolve and how they break. The wind is well documented as a major snow transport process (*e.g.*, Schmidt, 1980; Li and Pomeroy, 1997; Mott et al., 2010; Li et al., 2018). It creates cornices (*e.g.*, McCarty et al., 1986; Kobayashi et al., 1988; Yu et al., 2022) and mountaineers agree on the importance of wind in the formation of SBs. It is indeed unlikely that the creep affecting the top snow layers (Teufelsbauer, 2011)

is sufficient for a snow cornice (*i.e.* volumes of snow overhanging the crevasse and accreting from one or both lips of the crevasse) formed from the upstream lip of the crevasse to gather with the downstream lip, particularly on low angle glaciers. Therefore, only snowfalls under windy weather or wind-driven snow (Sokratov and Sato, 2001; Mott et al., 2010) are likely to allow the cornice accreting (Vogel et al., 2012), something that observational data should verify. Concerning the evolution of the SBs, it is likely that the opening/closing regime of crevasses has a critical influence on their stability. It is therefore necessary to appreciate/measure this regime, and more specifically the conditions of occurrence of crevasses in relation to the local bedrock topography. Finally, together with the regime of crevasses, it seems obvious that the meteorological conditions predominantly determine the periods of collapse either spontaneous or induced by the mountaineers, as in the case of snow avalanche (*e.g.*, Schweizer et al., 2003; Jomelli et al., 2007; Eckerstorfer and Christiansen, 2011) or cornice failure (*e.g.*, Vogel et al., 2012; Munroe, 2018; Hancock et al., 2020; Veilleux et al., 2021). This represents one of the major scopes of this paper under the form of an analysis of the results of two years of multiparameter monitoring of a crevassed site in the MBM.

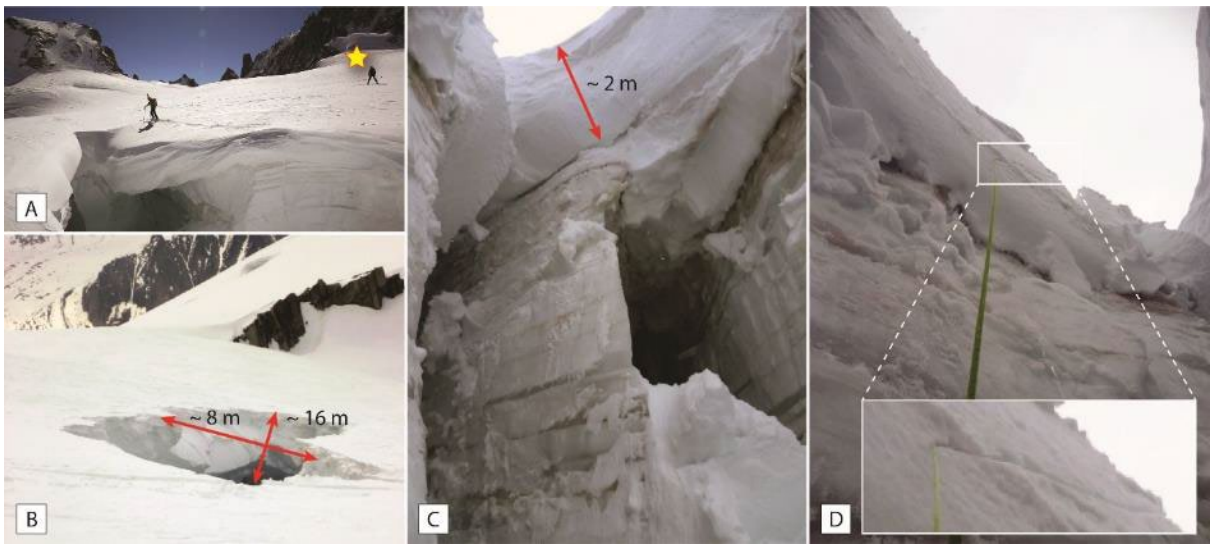


Fig. 1. An example of a fall into a crevasse in the Mont-Blanc massif (MBM) involving the failure of a large snow bridge (SB), near the Pointe Lachenal (3613 m a.s.l.), in April 2011 (ph.: B. Lapierre / F. Dominik). A: The area is known to be crevassed. Star: study site. B: Two roped-persons were following the visible footsteps of preceding mountaineers; one of them first put his leg through a hole immediately followed by the collapse of the entire SB over a distance of about 16 m. C: The thickness

of the SB at the edges was around 2 m. D: After a fall of about 10 m, the mountaineer came out unscathed after the rope had stopped his fall by getting caught in the lip of the crevasse.

## 2. Study area

### 2.1. Site requirements

The study required a site in the MBM massif answering several imperatives like: (i) being as representative as possible of the SBs that are subject to a marked accidentality, *i.e.* avoiding particular contexts (steep slopes which are least prone to falls as shown by Ogier et al. (2017), bergschrunds, etc.); (ii) being accessible all year round with a relatively short approach time, which reduced the possibilities to the Grands Montets area (3295 m a.s.l.) and the Aiguille du Midi (3842 m a.s.l.) both being reachable by cable-car; (iii) being permanently located in the glacier accumulation zone, leaving out the Grands Montets area which, during hot summers like 2003 or 2015, was found to be under ablation conditions; and (iv) being situated away from the main flows of climbers and skiers for safety reasons (reducing the risk of collision and stealing of equipment), thereby prohibiting several interesting areas reachable from the Aiguille du Midi.

A final difficulty was that glaciers have remained particularly snowy during the summer 2016 (set-up) due to massive snow falls during the preceding months of May and June. As a consequence, very few crevasses had lost their SBs. In view of all these elements, our attention was focused on a sector of the Col du Midi (3522 m a.s.l.), on the French side of the MBM (Fig. 2).

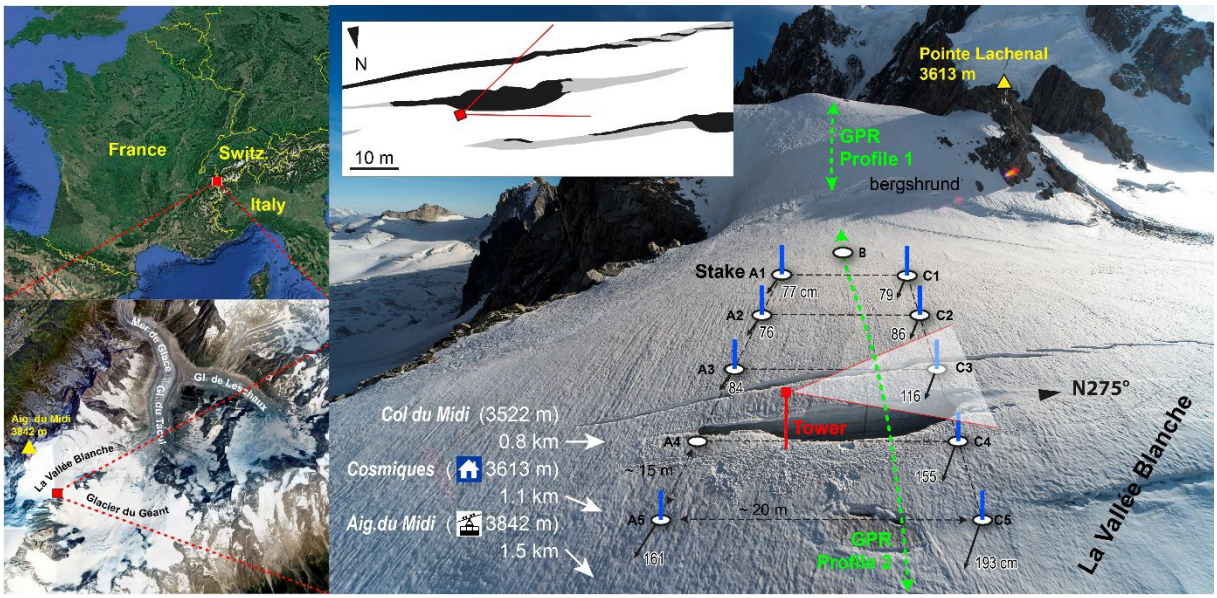


Fig. 2. Study site. Left: location (*Google Earth* images). Right: the site as on the 02 Sept. 2016 during the set-up (ph. drone E. Courcier). In red: position of the tower and the camera. In blue: stakes installed on the 02 April 2021 for the measurement of the glacier surface displacements; the values indicate the horizontal displacement computed between the 02 April and the 17 Sept. 2021 (5.5 months apart); the A4 and B stakes were not found. In green: GPR profiles. Insert: crevasse map of the 02 Sept. 2016 with collapsed SBs in black and SBs in place (minimum area) in grey. Altitudes are in m a.s.l.

### 2.2. Geographical and glaciological context

The crystalline MBM covers an area of 550 km$^2$ on the outer margin of the Western European Alps. Among the 82 summits ≥ 4000 m a.s.l. in the Alps, 28 are located there. Most of these belong to the watershed between the Rhône and Po basins. Excluding marginal glaciers such as ice aprons (Guillet et al., 2021), about 30 % (155 km$^2$) of the MBM area is covered by glaciers (Berthier et al., 2016) which are mainly slope and valley glaciers. 12 of the 94 glaciers of the MBM have an area of 5 km$^2$ or more (Gardent et al., 2014). The accumulation zone of some of these glaciers culminates at more than 4000 m a.s.l. explaining that their front then reaches low altitudes (1400/1600 m a.s.l.). The flow dynamics of the MMB glaciers have been the subject of numerous velocity measurements, using field or satellite data (Gagliardini and Meyssonnier, 1997; Vincent et al., 1997; Berthier et al., 2005; Trouvé et al., 2007; Fallourd et al., 2011) in order to better characterize the dynamics of temperate (ice at the pressure

melting point) and cold glaciers (ice below freezing point). Glaciological field measurements are also performed routinely on several nearby glaciers including the Mer de Glace and Argentière glacier (Vincent et al., 2009; Six and Vincent, 2014).

Our study area was precisely chosen on the wide ice-covered Col du Midi (3522 m a.s.l.) due to a large SB collapse which occurred a few weeks before the start of the monitoring. Our attention thus focused on a large crevasse (Fig. 2) located around 3450 m a.s.l., 1.5 km SSE of the Aiguille du Midi (about 45-60 min. walk), at the foot of the short (*c*. 50 m) ice and snow north face of the Pointe Lachenal (3613 m a.s.l.). Our study site is therefore located on the right bank of the *Vallée Blanche* glacier, in the glacier accumulation zone. Along with the glacier du Géant, it forms the glacier du Tacul, which then feeds (with the glacier de Leschaux) the Mer de Glace. The surface of the whole glacier area (*c*. 31 $km^2$) makes the Mer de Glace the largest glacier of the French Alps.

The set of crevasses is located on a smooth slope break. Upstream, a 100-m-long slope leads to the bergschrund of the Pointe Lachenal with a slope angle around 15°. It should be noticed that 62 % of the accidents documented by Ogier et al. (2017) occurred on slope angles between 5 and 20°. Downstream, the slope increases (20 then 25°) while, 250 m downstream, the ice from the surveyed area leaves the *Vallée Blanche* to feed the glacier du Géant through a densely crevassed diffluence pass (local ice acceleration). Ice velocities in our study site are not known as it is outside the areas covered by Trouvé et al. (2007), Fallourd et al. (2011) or Berthier and Vincent (2012). Berthier et al. (2005) calculated the horizontal displacement of glaciers of the MBM by cross-correlating SPOT 5 optical images between the 23 Aug. and 18 Sept. 2003, but the correlation coefficient is too weak in our area of interest. A stake located on the *Vallée Blanche*, 400 m NW of our study area, indicated a horizontal displacement of nearly 10 m over the period 11 Feb. 2015 - 23 Oct. 2015 (Réveillet et al., 2021).

### 2.3. Crevasse setting

During the set up on the 02 Sept. 2016, the largest crevasse – maximum width of 6 m at the ice surface, more than 70-m-long, and oriented W-E/275-280° – was discovered over a length of 37.5 m and a maximum width of 6 m (Fig. 2). A *Panocam* (wide angle camera) installed in spring 2016 at the top of the Aiguille du Midi showed that the SB that covered the crevasse had undergone a first collapse between the 27 and 28 July, a second one between the 30 July and the 01 of Aug. and then a strong enlargement over the period which preceded the monitoring (from the 26 Aug.). The crevasse was 17-18 m deep. At the bottom, the narrowing was filled by the previously fallen SB.

5 m upstream from the upper lip of the main crevasse, another crevasse, a few tens of centimetres large, appeared over a length of 90 m. 7 m downstream from the lower lip of the main crevasse, a third crevasse was present. Locally larger than 4 m, a large part of it was still covered by a SB. This type of crevasse pattern is visible each year, when SBs are collapsed or when they form depressions on the glacier surface. To study them, we focused during two years on monitoring weather parameters and evolution of the SB. We have also inferred some glacial parameters such as thickness and surface velocities.

## 3. Methods

### 3.1. Detailing the glacial context

Ground-penetrating RaDAR (GPR) is widely applied to study glaciers (see for instance the excellent and exhaustive description of S. A. Arcone in Jol, 2008) and particularly appears to be a valuable tool for measuring the thickness of mountain glaciers and investigating the internal structure and fracturing of glaciers through flow properties (Woodward and Burke, 2007; Fischer and Kuhn, 2013). The method is based on the fact that changes in dielectrical permittivity, *e.g.* at material boundaries like ice/rock interface, lead to a partial reflection of the signal (van der Veen, 1998). A GPR survey was carried out on the 02 April 2021 (Fig. 3A and 3B) to image the ice thickness and the bedrock topography (Fig. 4A)

with a 100 MHz antenna along a 150-m profile between the top of the Pointe Lachenal north face and the bergschrund (Profile 1) and between the bergschrund and few tens of meters downstream of the monitored crevasses (Profile 2, see Fig. 2). In order to account for the presence of firn overlying deeper ice, an overall velocity of 0.18 $m.ns^{-1}$ was chosen to map the double travel times into depths.

Because they similarly induce a material contrast (between air-filled fractures and surrounding ice) crevasses are also potentially detectable by GPR, a property used for detecting hidden crevasses along several ground traverses in Antarctica and Greenland (Delaney et al., 2004; Arcone et al., 2016; Marsh et al., 2021). Their main signature usually consists of local reflection from the walls themselves or from specific sharp features along them, leading to a set of superposed hyperbolae (Zamora et al., 2007; Eder et al., 2008). Despite the contrast in physical properties between snow and ice, snow-filled crevasses yield a much less clear signal probably due to an incomplete filling leaving many voids of chaotic geometries responsible for noisy signals. Besides, the signal rapidly degrades as one deviates from the ideal crossing of the crevasse at a right angle (a parallel GPR profile will at the best provide constant reflectors that are almost impossible to interpret as crevasses). This is one of the main limitations in the efficiency of real-time GPR systems mounted ahead of vehicles in order to detect crevasses on the way.

GPR power of resolution (minimum distance between two nearby reflectors for them to be separately detected) is theoretically given by the Raileigh criterion of $\lambda/4$. Due to the pulse width, this criterion once enlarged to $\lambda/2$ can generally also be considered as the radar overall accuracy (Le Meur et al., 2018), meaning that in the present case, with a velocity of 0.18 $m.ns^{-1}$ and an antenna centre frequency of 100 MHz, an accuracy of some 90 cm can be reached in the proposed derived depths.

A second set of antennas (200-MHz unshielded bistatic antennae) was also tested so as to provide twice as high an accuracy in the measurements (around 45 cm). Unfortunately, GPR is all the more sensitive to noise as the central wavelength $\lambda$ is close to the characteristic size of perturbating objects like voids, irregularities along crevasse walls, etc. As a consequence, the signal was even more noisy, therefore precluding proper localization of buried crevasses.

In parallel, a Real Time Kinematic (RTK; Fig. 3C) set of three GNSS geodetic receivers was set up for two purposes. The aim was first to accurately geolocate the different GPR profiles and secondly to provide both an accurate DEM of the ice upper surface and the displacement field of a stake network. After setting up a base station on a known geodetic point (see Fig. 2), a second receiver was mounted on the GPR so as to provide the position of every RaDAR trace with an estimated accuracy of less than 10 cm.

The third receiver was then dedicated to monitor the glacier upper surface. The upper snow topography was accurately (5-cm accuracy) measured over some 124 points later interpolated to produce a Digital Elevation Model (DEM) of the study area (Yang et al., 2019).

Moreover, in order to analyse the movements of the glacier, we installed (Fig. 3D) 11 2.3-m-long wood stakes vertically on the glacier (1 m within the snow, 1.3 m emerging) whose positions were then accurately measured by RTK dGNSS. Downstream of the bergschrund, a first stake B was placed. Then, two parallel lines (A and C; Fig. 2), each consisting of 5 stakes 15 m apart (*i.e.*, lines of about 60 m), were laid out along the line of steepest slope with a spacing of 20 m. The stake line A was located a hundred meters from the right bank of the glacier; the line C was set in a slightly more central position on the glacier.

Fig. 3. Field campaign of the 02 April 2021. A: GPR measurement with a 100 MHz antenna (Profile 1). One operator pulls the 6-m long antenna with the GPS antenna exactly located half way between the emitter and receiver parts of the GPR. The second operator checks for proper GPR data acquisition on the computer with a dedicated software. A third one is often necessary to ensure correct positioning of the antenna on the ground. B: idem (Profile 2). C: dGNSS survey to create a DEM of the glacier surface and precisely locate the 11 wood stakes (insert: installation of the GNSS base station); D: stakes implantation using a perforator and a snow drill.

Radargrams were post-processed with the *ReflexW* software (Sandmeier, 2004) including: (i) correction for time zero, (ii) background removal (removing uniform spurious reflectors, reducing ringing), (iii) energy decay gain function to compensate for the energy geometrical loss, and (iv) various low-pass filters to specifically reduce noise. Altitudinal profiles along GPR profiles were used for a topographic migration of the data allowing for a correct repositioning (and dipping) of the reflectors (see Fig. 4). If the post-processing appeared useful for revealing the bedrock structure (Fig. 4A), it is clear that the antennae used for investigating the narrower snow (and crevasses) was less appropriate and only allowed for locating the crevasses along the bedrock profile (Fig. 4B) without allowing a detailed view of their inner structures as was the case with more dedicated GPR studies (*e.g.*, Eder et al., 2008; Singh et al., 2013). Higher frequencies (ideally from a 500-Mhz antenna) should allow for more details in the structure provided. The signal to noise ratio can be increased by stacking more traces when triggering over much shorter distances (for a higher spatial resolution as the one we could afford over a limiting single day survey).

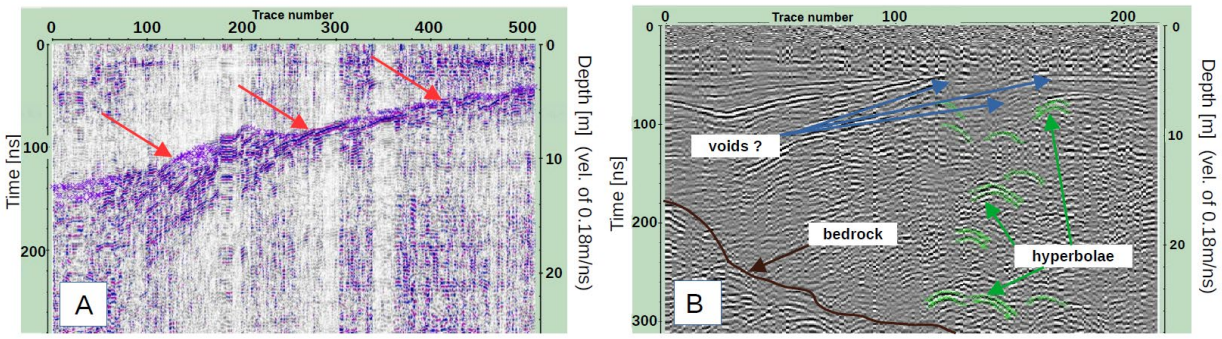

Fig. 4. Portions of GPR profiles acquired with a 100 MHz antenna. A: Detail of Profile 1 showing the ice/rock interface (red arrows) where ice thickness ranges between 4 and 12 m. B: Detail of Profile 2 showing the probable presence of two nearby crevasses expressing under the form of hyperbolae (or branches of hyperbolae). Also visible are possible voids (lack of reflection) that could indicate cavities under the SBs.

### 3.2. Parameter of interest and sensors used for the two-year monitoring

The monitoring system (Table 1), acquiring data hourly, was composed of high-performance sensors to meet the environmental constraints. It included a vane anemometer and a snow height measurement system (here, a reference acoustic system; Augros and Zanghi, 2008). In addition, a *Flowcapt* snow transport measurement system measuring solid particle flux intensities and wind speeds (average per 15 min period) had to be used (Chritin et al., 1999; Xie et al., 2021). Associated with these sensors is an automatic camera tracking the evolution of the SBs every 2 h, as it has been done in the case of cornices along a ridge by Munroe (2018) or Veilleux et al. (2021). Initially, a second camera was meant to be installed in the crevasse to monitor the SB construction from a low angle but this appeared impossible because of the repeated snowfalls. A sight present in the field of the camera was necessary to give a scale to the elements identified and to be measured thereafter on the photos. This sight was also designed to facilitate the focusing of the camera in unfavourable conditions (snow, fog).

Once the SB is built, the snow layers constituting it can be affected by different metamorphisms (Colbeck, 1982), especially those related to outside temperatures (melt metamorphism), the solar radiation intensity, and the temperature gradient between the air inside and outside the crevasse (temperature gradient metamorphism), which can lead to an increase or, on the contrary, to a reduction in the strength of the SB, similar to what is known about the stability of snow packs (Wever et al., 2016; Wiese and Schneebeli, 2017). The temperature of the outside air (measured in a cup shelter with natural ventilation approx. 5.5 m above the snow surface), inside air (in the crevasse at depths of -5 and -10 m), and at different depths in the snow (-1, -3 and -5 m), as well as the amount of

solar energy received (pyranometer) were therefore to be measured (Table 1). Finally, in the crevasse, a potentiometric wire extensometer was used to monitor the evolution of its opening (time-dependent width) as the width of the crevasse undoubtedly modulates the mechanical properties of the SB. Snow characteristics (density, wetness, grain size and shape) have sadly not been registered.

| **Material / Sensor** | **Manufacturer** | **Model** | **Units** | **Accuracy** | **Operational range of operation** | **Initial height / snow surface (m)** |
|---|---|---|---|---|---|---|
| Anemometer - wind vane | *Young* | 05103 | m/s | ± 0.3 m/s | 0 to 100 m/s | +7.2 |
| Acoustic snow meter | *Campbell* | SR50A | cm | ± 1 cm | 0,5 to 10 m | +5.8 |
| Snow-drift/blowing | *ISAW* | Flowcapt FC4 | g/m$^2$/s | ± 5-10 % | Up to 250 g/m$^2$/s | +0.5 |
| Digital automatic camera (10 MP) | *Canon* | 1000D | / | / | / | +5.8 |
| Camera lens | *Canon* | EF-S 18-55 mm | / | / | / | / |
| Sight (alu. mason ruler) | *Definor* | 2 x 4 m | / | / | / | 0 to -8 |
| Temperature sensors | *Campbell* | 107 | °C | ± 0,2°C | -35 to +50°C | -5 and -10 |
| Pyranometer | *Apogee* | SP-110 | kW/m$^2$ | ± 3 % | 0 to 2 kW/m² | +7.2 |
| Wire extensometer | *Scaim* | PT9101 | cm | ± 0.25-1 % | Up to 15 m | -4 |
| Logger | *Campbell* | CR1000 | / | / | -25 to +50°C | 4.5 |
| Aluminium tower 7 m | *Campbell* | UT20 | / | / | / | / |
| Battery | *Yuasa* | 22 Ah | / | / | / | 4.5 |
| Solar panel | *BP Solar* | 30 W | / | / | / | 5.5 |

Tab. 1. Equipment and sensors used to monitor the crevasse and the SB.

### 3.3. Set-up and maintenance

A 1.2 m deep hole was then dug in the snow, immediately downstream of the main crevasse, to anchor the 7-m-high aluminium tower that would support most of the elements (Fig. 5). This height was chosen to have a large angle view for the camera and to limit the risks of burying the equipment in the snow because mass balance surveys indicate accumulations of 4 to 7 m of snow in the area of the Col du Midi (Réveillet et al., 2021). The assembly of the tower, its ancillary elements, and all the other instruments was carried out on the site. The tower was stabilized by 4 cables fixed on 'dead anchors' in the snow. A 5-m-deep vertical borehole was drilled in the snow to install three temperature sensors

(at depths of 1, 3, and 5 m) with a *Heucke Ice Steam Drill* (Heucke, 1999). Another drilling connecting the foot of the tower to the interior of the crevasse was done to receive a sheath in which the cables necessary for the internal instruments were passed. A whole day was finally necessary for the main part of this set-up (https://youtu.be/sO1Y4BwyR8A).

Every two-months control visits (checking of the tension of the cables, verticality of the tower and orientation of the camera, snow removal from the equipment, etc.) and data collection were undertaken. Sometimes, they allowed the installation or removal of extra sensors: installation of the extensometer (01 Dec. 2016), adding of the maximum wind velocity (same device as for the mean speed) (29 March 2017), installation of the *Flowcapt* (01 June 2017), removal of the extensometer before it was no longer accessible due to the likely closure of the crevasse (01 June 2017), etc. On the 01 June 2017, the tower was also moved 6-7 m upstream due to glacier movements. It has been relocated immediately upstream of the new main crevasse. Sometimes, like for the installation of the extensometer on the 01 Dec. 2016, or for the removal of the snow above it on the 30 Jan. 2017, access to the interior of the crevasse required digging a hole in the SB, allowing to appreciate its structure. Maintenance during the end of the first year and during the second year was more difficult. After a period of intense melting in July 2017 – including high altitudes –, the anchors of the cables came out of the snow and the tower collapsed. It was reinstalled on the 30 July 2017. The Eleanor storm of 02-03 Jan. 2018 (extratropical cyclone and windstorm that affected western Europe; Möller et al., 2018) again brought the tower down and broke several sensors that could not be replaced even after the tower was put back in place (12 Jan. 2018). Finally, the August 2018 heat wave gradually caused the tower to topple and ultimately fall. The entire system was evacuated on the 22 of Aug. 2018. During these two years, the observation by the keepers of the Cosmiques hut and the *Panocam* of the Aiguille du Midi were useful to remotely check the state of the tower.

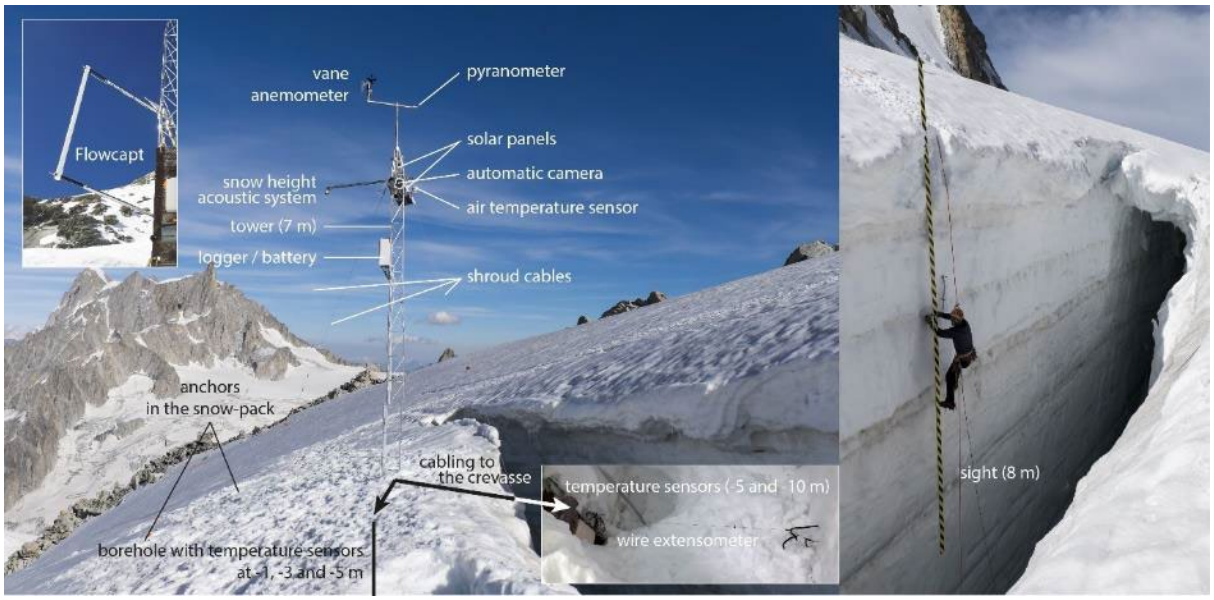


Fig. 5. The monitoring system (ph.: E. Courcier) on the 02 Sept. 2016. The *Flowcapt* (upper left) and the extensometer (bottom) were installed later. The extensometer was fixed on one side to a board screwed in the ice for the one side and to a lunula in the ice for the other side. Right: installation of two 4 m sights.

### 3.4. Data analysis

Images from the camera were first selected according to their usability (correct visibility and adequate view angle). 27 % of the study period is not covered by usable images, mainly during the second year (see Fig. 7). A time-laps tool software (timelapsetool.com) was used to highlight the SB construction-evolution-failure phases from the images. *ImageJ* (Schneider et al., 2012) and a plugin generating contour lines was utilised for failures to artificially accentuate snow edges on pictures (see Fig. 15).

The meteorological data were analysed using Python programming language. To understand specific weather events during SB construction and failure phases, additional data from the Aiguille du Midi (*Météo France* weather station), from a nearby weather station (Requin hut; 3 km away from the study site), or from archives of the AROME meteorological model (run 0Z), a small-scale numerical prediction model used by *Météo France* (Seity et al., 2011), could also be used. It is to note that the automatic camera also provides supplementary general weather information, useful for understanding the ongoing processes (see *e.g.*, Vogel et al., 2012).

## 4. Results

### 4.1. Geometry and movements of the glacier

GPR measurements revealed an ice/firn thickness varying from *c*. 4 m in the top part of the Profile 1 to more than 35 m in the lower part of the Profile 2 (Fig. 6). It can be noted that when the instrumentation was set up, the 18 m depth of the crevasse only intersected firn, which is consistent with Gillet et al. (1976) who found ice at 35 m during a coring completed in 1971 a few hundred metres from our study site. Together with the dGNSS data, GPR data allowed to reconstruct the bedrock topography (Fig. 4B). The average slope of the bedrock along the 150 m profile is 35°. The profile presents a slight hump in the middle and a more pronounced one below the smooth break in slope on which the crevasses studied appear. Two crevasses are recognized in this sector while another crevasse appears at the level of the slight hump. The bergschrund, clearly identified visually, is not covered by the GPR data.

dGNSS measurements at the stakes have been carried out on the 02 April and repeated on the 17 Sept. 2021, covering a period of 5.5 months. Two stakes were missing: stake A4 was probably implanted on a SB that collapsed in Aug. 2021 while stake B was probably swept away by a snow avalanche that occurred on the 20 June 2021. Measurements indicate horizontal displacements between 76 ± 6 and 193 ± 6 cm (Fig. 2 and 6) with an average displacement of 114 cm, *i.e.* an average velocity of about 2.5 $m.a^{-1}$ (min.: 1.66 $m.a^{-1}$; max.: 4.21 $m.a^{-1}$). The middle of the glacier is faster with surface velocities between 5.9 and 13.9 $m.a^{-1}$ measured at five stakes by Réveillet et al. (2021). All these very low speeds suggest the behaviour of a still cold glacier (< 0°C) which is partly confirmed by measurements of the ice temperature into the crevasse made in Sept. 2016 (-0.3 to -1.5°C while the surface snow was at this time of the year at 0°C).

Overall, we note an acceleration of the glacier surface velocities from upstream to downstream with an increase over 60 m of +209 % for stake line A and +245 % for line B (Fig. 2). Line B accelerates more due to its more internal position on the glacier (*e.g.*, Berthier et al., 2005; Fallourd et al., 2011) while the glacier dynamics is already affected by the turn located downstream (diffluence). The shift in the orientation of the glacier from NNE to SE is indeed indicated by the orientation of the movement of the stakes: 43.7°, *i.e.* nearly 40° more than the direction orthogonal to the studied crevasses.

The acceleration is not uniform longitudinally either. Looking at the complete line B (no stake loss), the acceleration is initially reduced on the first (upper) 15-m-long section (+0.15 $m.a^{-1}$), then strongly accelerates on the next 15-m-long section (+0.65 $m.a^{-1}$). The acceleration is then homogeneous on the last two sections: +0.85 and then +0.83 $m.a^{-1}$. In its lower part, the second section covers the zone where the crevasses open. The strong acceleration between the first and second sections is probably partly related to this opening crevasse, immediately upstream of the subglacial hump (Fig. 6). Crevasses are closing in area of the third and fourth sections with similar acceleration values.

This rheology is also expressed by the opening/closing dynamic of the crevasses which is recognized both from photos taken from the tower (Fig. 7) and from the extensometry data that indicate the pacing of the closure of the crevasse (Fig. 8).

Over the two years of monitoring, the camera took 2840 photos. During certain periods, there was no photo or the photos were not usable (bad orientation of the camera, bad weather, presence of ice or snow on the protection case of the camera) (Fig. 7). 2363 photos are hence usable allowing to identify 3 generations of "main" (most widely opened) crevasses as well as their behaviour (opening/closing). From the start of the monitoring in Sept. 2016 and during the following autumn (Period A on Fig. 7), three crevasses were observable: a main one (**1** on Fig. 7), which was up to 6 m wide, and two others of smaller width on each side (including the upper crevasse **2**). Crevasse **1** remained identifiable for most of the winter 2017 because of a depression on the surface of the SB, or even a small drop-off at the upstream lip of the crevasse. During spring 2018, the camera was able to survey the opening of crevasse **2** while crevasse **1** continued its closure (Period B). The extensometer was installed between

the 01 Dec. 2016 and the 01 June 2017. In Jan. 2017, the cable got stuck in the snow pack (fallen from the SB or wind-driven) before it was cleared on the 30 Jan. 2017. Despite this, it recorded a closure of 68.5 cm, *i.e.* 0.37 cm/day. Initially rapid in Dec. 2016 (0.92 cm/day) and probably faster in Nov. 2016 (modelled 2.7 cm/day), this closure was then much slower (0.013 cm/day between Jan. and May) with an inflection point occurring on the 13 April 2017 (Fig. 8). After this date, the closure is only 1.5 mm in 1.5 months, probably due to the compressed mass of snow into the crevasse preventing further closure. Two measurements of the width of crevasse **1** were manually made at a location close to the extensometer: 4.25 m on the 02 Sept. 2016 and 1.45 m on the 01 June 2017, *i.e.* a width difference of 2.8 m meaning an average closure rate of about 1 cm per day, which is consistent with the previous results. Photographs suggest an equivalent opening rate for crevasse **2**. Period C corresponds to the appearance and opening of crevasse **3** while crevasse **2** was closing.

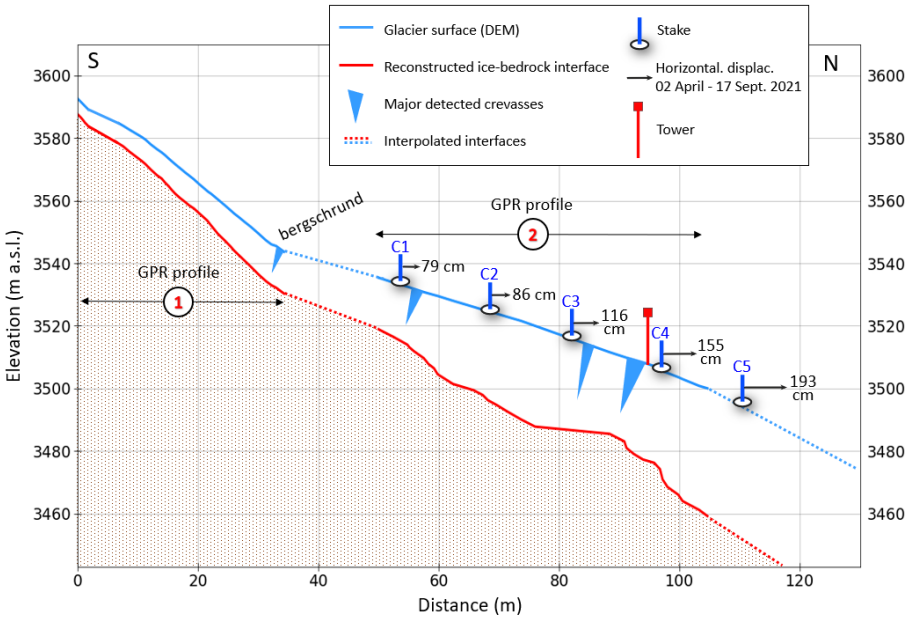


Fig. 6. Profile of the bedrock and glacier in the study area. Three main crevasses can be positioned from the GPR profiles. The bergschrund, clearly visible on the glacier, is reported without having been identified from the measurements (no GPR data).

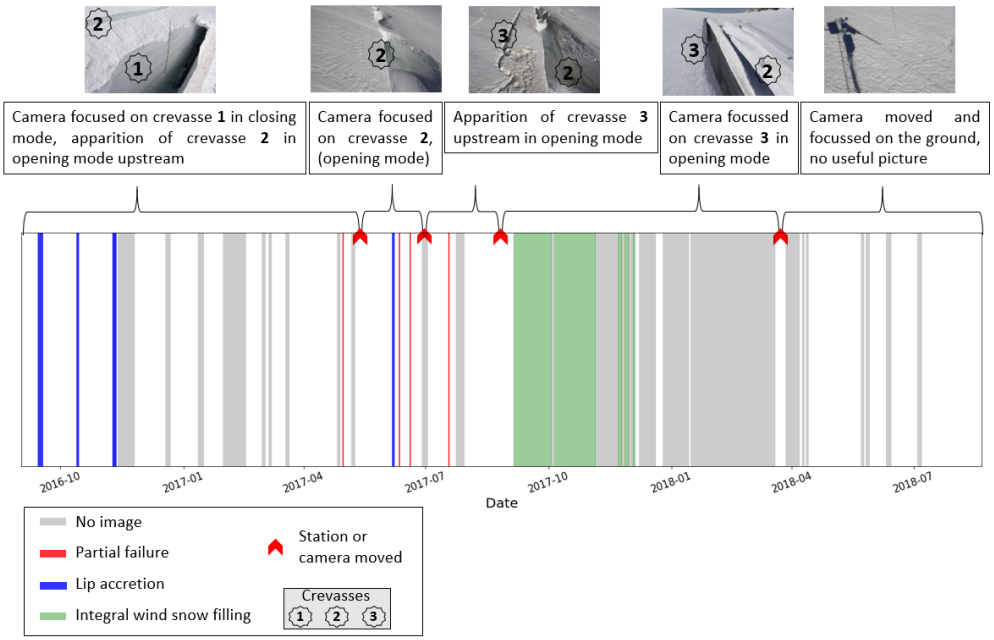


437

438 Fig. 7. Evolution of the usability of the photos, crevasse system life and major events over the whole monitoring period. White

439 periods: no significant change.

440

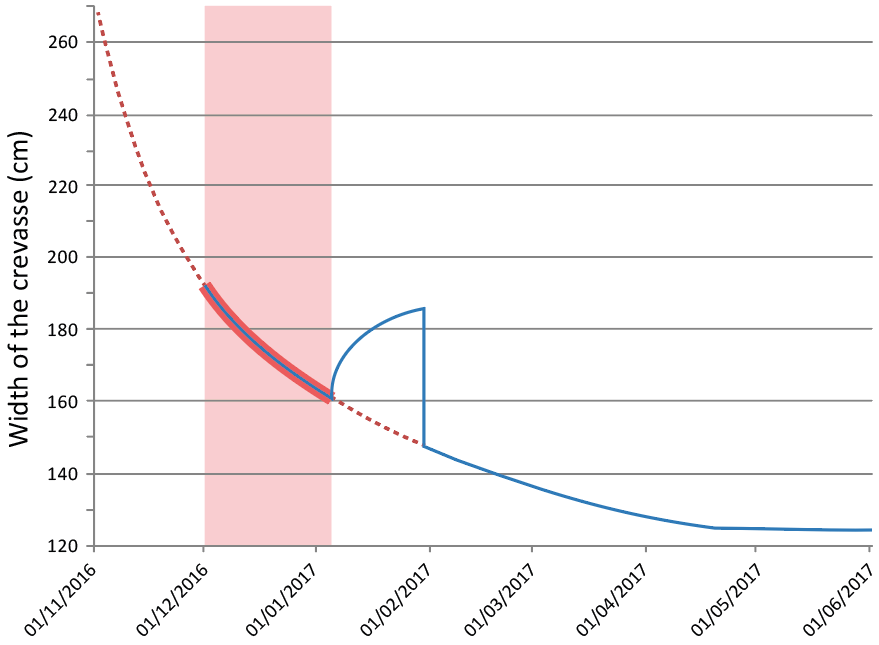


441

442

443 Fig. 8. Evolution of the width of crevasse **1** over the period Nov. 2016 – May 2017. In blue: measurements made with the

444 potentiometric extensometer placed in the crevasse. In Jan. 2017, the curve shows an aberration linked to the cable of the

extensometer stuck into the snow. Red dotted curve: polynomial fit adjusted ($R^2$ = 0.9999) on the Dec. 2016 measurements (thick red line).

### 4.2. Meteorological parameters

The mean annual air temperature is slightly contrasted between the first (03 Sept. 2016 - 31 Aug. 2017) and second year of monitoring (01 Sept. 2017 - 22 Aug. 2018), with -4.5°C and -5.9°C respectively, the 2017-18 winter being colder than the previous one (Fig. 9). Minimum and maximum air temperatures were respectively -25.6°C (16 Jan.) and +16.0°C (11 June) in the first year, and -28.1°C (28 Feb.) and + 11.7°C (19 June) in the second year. At a depth of *c*. -3 m and -5 m in the snow, the average firn temperature for the period 3 Sept. 2016 - 31 May 2017 was -5.3°C (temperatures between 0.0°C and -9°C) and -1.8°C (between 0.0°C and -5°C), respectively. Together with the low velocities measured at the glacier surface, the temperature of the ice within crevasse **1**, the modest thickness of the glacier in the study area, the permafrost context in all the surrounding rock walls (Magnin et al., 2015), these subsurface temperatures suggest the still cold state of the glacier at the location of the study crevasses. In the crevasse **1**, the average air temperature over the same period was -1.8°C at -5 m and -1.0°C at -10 m but these data are not usable because the sensors were quickly caught in thermally insulating snow. This unfortunately prohibits a number of analyses concerning the metamorphism of the snow constituting the SB of crevasse **1**. In any case, the relocation of the monitoring system performed on 01 June 2017 led to the end of the temperature data acquisition in the snow and within the crevasse.

The diurnal values of solar radiation measured by the pyranometer vary strongly between winter (values close to 0 $kW/m^2$) and summer when the values were able to rise to an hourly mean of 1. 2 $kW/m^2$ and an hourly total of 21.6 $MJ/m^2$ on the 03 July 2017 at 12:00 UTC. The snow height data were unusable as values are inconsistent or unrealistic with precipitation data from other weather stations and observations made during field trips. Observations at the tower during each visit indicate sub-meter changes in snow thickness in the winter but noticeable melting in the summer, resulting in July

2017 as well as Aug. 2018 in the fall of the tower after the melting of the snowpack around the base of the tower and at the anchors of the cables. During winter, the wind seems to erode/transport most of the snow that is deposited. The *Flowcapt* has operated properly for two periods that were too short to corroborate this observation and this makes the snow transport data also useless. Potentially significant wind transport of snow is, however, strongly suggested by the wind data (Fig. 9). Average velocities were recorded over the period 2 Sept. 2016 - 07 Jan. 2018 (mean: 5.4 $m.s^{-1}$; max. : 24.7 $m.s^{-1}$ on 03 Jan. 2018 during the Eleanor storm, followed by 23.1 $m.s^{-1}$ on 14 Dec. 2017) and maximum velocities over the period 29 March 2017 - 07 Jan. 2018 (mean: 10.2 $m.s^{-1}$; max. 56.2 $m.s^{-1}$ on the 03 Jan. 2018 during the Eleanor storm, followed by 42.7 $m.s^{-1}$ on the 14 Dec. 2017). From the orientation point of view, these are mainly westerly winds (Fig. 10).

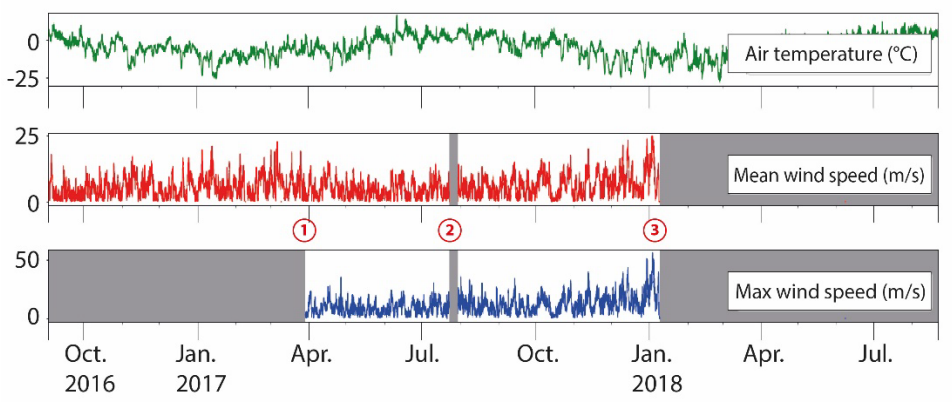


Fig. 9. Time-dependency of outside air temperature and wind average (15 min.) and maximum speed. 1: add of max. wind speed (29 March 2017); 2: fall of the tower (23 July 2017) and reinstallation (30 July 2017); 3: Eleanor storm and fall of the tower (07 Jan. 2018).

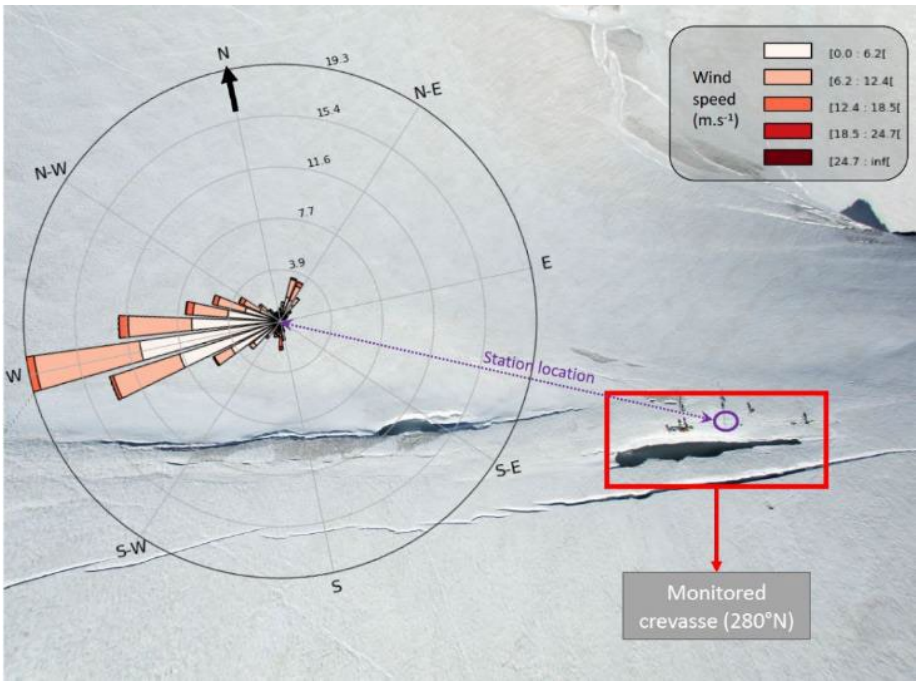


Fig. 10. Wind at the study site during the period 5 Sept. – 5 Dec. 2017. The concentric circles represent the percentage of the wind dataset.

### 4.3. State of the snow bridges

We deplore several periods with no available images due to snow and ice on the protection box of the camera, bad weather, or movement of the camera leading to wrong targets (Fig. 7). However, with the analysis of the remaining usable images, the following events could be identified:

- 2 main lip accretion events: from the 09 to 11 Nov. 2016 (after two first cases on the 13-15 and 23-27 Oct. that concerned a small western cornice developing, parallel to the crevasse, from the SB which did not collapse) which ended up with an entire hiding of the crevasse by a complete SB formation (Fig. 11; Tab. 2) and, to a lesser extent, a similar event from the 05 to the 07 June 2017.
- Several periods of snow filling of the crevasse (including those of Tab. 2), and a succession of fillings eventually leading to an integral crevasse filling, without any lip accretion, from the 05 Sept. to the 05 Dec. 2017.
- 4 partial failures on the 01 May, 12 and 20 June, and 18 July 2017.

| Date | Wind speed (mean) | Wind dir. (mean) | Temperature | Process |
|---|---|---|---|---|
| 02 Sept. - Oct. 13 | Moderate (3.9 $m.s^{-1}$) | S to W (225°) | -9 to +6°C | Slight deformation (creep) of the surface snow constituting the upstream lip of the crevasse |
| 14-24 Oct. | Moderate (4.7 $m.s^{-1}$) | S to W (229°) | -10 to 0°C | Light wind snow filling (WSF) of the crevasse |
| 25 Oct. - 01 Nov. | Moderate (4.9 $m.s^{-1}$) | W (269°) | -1 to +3°C | Continuation of the WSF |
| 02-09 Nov. | Strong (7.3 $m.s^{-1}$) | W (272°) | -8 to -18°C | Very important WSF (c. +3.5 m of snow at the bottom of the crevasse) |
| 9-11 Nov. | Very strong (10.6 $m.s^{-1}$) | N to W (311°) | -11 to -15°C | Construction of the SB |

Tab. 2. Weather parameters and snow structures formed during the autumn 2016, until the complete first SB was built.

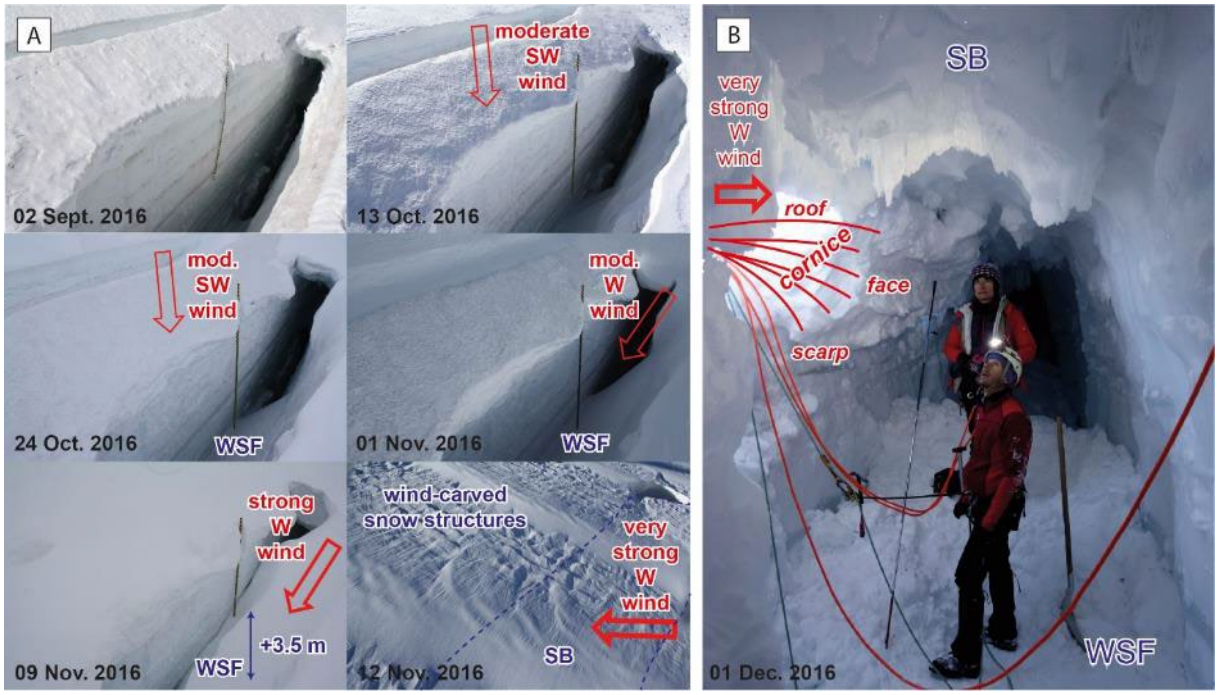


Fig. 11. The SB during the autumn 2016. A: Evolution of the crevasse between the 02 Sept. and 12 Nov. 2016; B: the cavity existing between the wind snow filling (WSF) and the SB as well as the hole dug to penetrate under the SB allowing to observe the typical structure of a cornice that experienced accretion.

## 5. Discussion

### 5.1. Two different types of snow structures depending on wind direction

The structure built in November 2016 corresponds to a cornice accretion (see *e.g.*, Eckerstorfer et al., 2013) from the downstream lip (northern one) as evidenced by the large cavity discovered during the 01 Dec. 2016 visit between the top level of the WSF and the bottom of the SB, as well as the SB structure (Fig. 11). The hole dug in the SB (Fig. 11B) showed a structure made of successive cornices from the downstream lip of the crevasse, similar to what is observed in high latitude regions for cornices that grow by extending leeward as a sub-horizontal slab and by depositing windblown snow particles (snow sintering and bond formation; Herwijnen and Miller, 2013) on a cantilever slab, notwithstanding the behaviour of eddies on the leeward of a mountain ridge (Kobayashi et al., 1988; Eckerstorfer et al., 2013). Due to bad weather during the 09-11 Nov. 2016 event, the photos are not usable and do not allow to know whether the SB was built over a short time (few hours) or whether two days were necessary. In Svalbard (Norway), Hancock et al. (2020) measured cornice accretion rates of 10 $mm.h^{-1}$ during several accretion events coinciding with winter storms. It is therefore possible that the two days or so were needed to achieve the SB in our study site.

When snow is available (precipitation or remobilization), a strong wind parallel to the crevasse oriented 275°N (W wind) allows to fill it, while a crosswind (*e.g.* NW wind on 09-11 Nov. 2016) allows a SB to form by cornice accretion until the structure reaches the opposite lip. The formation of the SB required mean wind speed of 10.6 $m.s^{-1}$, which is consistent with the results of Voguel et al. (2012) showing that mean wind speeds around 12 $m.s^{-1}$ can build cornices. The second construction event of a SB by cornice accretion is less spectacular; it took place on the 05-07 June 2017, under cold temperatures (mean: -6.7°C) with a strong wind (max. speed up to 20 $m.s^{-1}$). But, coming from the W (mean: 364°), only a small cornice accretion parallel to the crevasse occurred. The strong wind allows to reach the force required to eject the snow particles (Pomeroy and Gray, 1990) while the weak cohesion of fresh snow gives it a high potential mobility index (Naaim-Bouvet et al., 2012). This is why all the accretion events observed in our study occurred either during snowfall events or the following days according to *Météo France* data.

543 During the period 02 Sept. - 12 Nov. 2016, we were able to distinguish two categories of processes
544 through the analysis of the images from the monitoring system: accretion phases (204 hours) and non-
545 accretion phases (1637 hours) some of which being WSF. Figure 12 shows that the wind during this
546 period was mainly oriented in a direction close to the crevasse direction: 60 % of the dots are inside a
547 ±20° buffer zone around the direction 275°N (non-accretion phases). At the scale of the Mer de Glace
548 basin, with dominant winds also mainly coming from the West, more than 4 $km^2$ of glacier surface
549 within which the crevasses are mainly oriented W-E could be preferentially affected by WSF. For
550 accretion phases (black dots on Fig. 12), more than 75 % of the sample are outside of this buffer zone.
551 This confirms that accretion is predominant when wind direction creates a significative angle with the
552 crevasse (around 40° and 310°) as it has been described for cornices at high latitude (Kobayashi et al.,
553 1988; Vogel et al., 2012; Eckerstorfer et al., 2013).
554 In addition, Figure 13 shows that 50 % of the mean wind speed values during accretion events were
555 higher than 7,8 $m.s^{-1}$ but it remains hard to find a wind speed threshold because of a lack of data (an
556 image every 2 hours) and also because some other factors like the air temperature can be involved.
557 Contrary to the finding of Vogel et al. (2012), cornice accretion seems here to be influenced by air
558 temperature: 75 % of the accretion events took place with temperatures between -2,3 and -12,3°C,
559 which correspond to globally lower temperatures than for the non-accretion events. This could be
560 explained, at least partly, by the fact that melting by friction – which facilitates accretion – is likely and
561 paradoxically more efficient under low temperatures (Latham and Montagne, 1970).
562 Before the period 9-11 Nov. and the construction of the SB, the wind parallel to the crevasse made
563 WSF efficient but not lastingly enough to fill the entire volume of the crevasse that can be estimated
564 to *c*. 3000 $m^3$ from the dimensions measured on the 02 Sept. 2016. An integral filling means no SB
565 structure – but a snow wedge – and therefore no risk of failure and no risk of fall for practitioners.
566 During the monitoring, only one integral filling of the opening crevasse **3** (see Fig. 7) has been observed.
567 This unexpected process took place between the 05 Sept. and the 05 Dec. 2017. Besides the direct
568 snowfalls, it is explained by the snow transport and the preferential deposition into the crevasse acting

569 as a topographic depression that traps the wind flow, causing a decrease in snow-carrying capacity
570 (Lehning et al., 2000; Lehning and Fierz, 2008; Prokop and Procter, 2016). Westerly winds are
571 predominant in our study area (Fig. 10): 71 % of the winds during this period were NW to SW and 19,3
572 % of the winds were oriented 270°N ±5, which is almost the same orientation as the crevasse. This
573 prevalence of westerly winds, due to the synoptic wind pattern on the French side of the MBM and
574 the presence of the Col du Midi (Réveillet et al., 2021), together with sufficient speeds for fresh and
575 dry snow transport, explains this preferential WSF instead of cornice accretion. This is corroborated by
576 the threshold for dry snow transport ranging from 4 to 11 $m.s^{-1}$ (Li and Pomeroy, 1997) associated to a
577 mean wind speed of 6.0 $m.s^{-1}$ during the period 05 Sept. - 05 Dec. 2017.
578 Observations made in recent years on the MMB glaciers confirm the occurrence of the two types of
579 structures presented above. The collapse of a SB or the crossing of a crevasse by another one often
580 allows the observation of the profile of these structures. However, when a crevasse reaches a certain
581 stage of closure, it may be difficult to know whether the compressed snow/ice filling of the crevasse
582 corresponds to an SB formed by cornice accretion or a WSF. In addition, a third type of structure can
583 be identified, corresponding to a SB formed by bonded/sintered snow along with the progressive
584 opening of a crevasse (Fig. 14). A first SB forms above a narrow crevasse due to the cohesion of the
585 snow and then fractures as the crevasse continues to open, while a new layer of snow again masks the
586 crevasse, and so forth.
587 In many cases, it can also be a question of "mixed" structures: a deep SB forms according to the third
588 mode using the asperities of the crevasse walls and above which a WSF will built up, a collapsed or
589 collapsing SB wedged between the crevasse walls and above which the snow redeposits, etc.
590 For the practitioners' safety, crevasse closing contexts tend to increase the resistance of the SBs
591 (compaction, increase in sintering level of the snow) while opening contexts tend to fracture the SB,
592 thus weakening it and favouring its failure. In addition, once a SB is formed as it was the case during
593 the fall 2016, the images from the camera allow to highlight some SBs/crevasse presence field clues:
594 (i) apparition of various successive wavelets following the lip of the crevasse and making small steps in

595 the direction of the crevasse, (ii) changes in the snow-deposition features (small snow dunes, sastrugis,
596 etc.), (iii) changes in the snow aspect (colour, grain size) above the crevasse (probably due to a different
597 snow metamorphism related to the presence of a cavity under the SB), (iv) possible detection of cracks
598 in the snow (see also Eckerstorfer et al., 2013) at the edge of the crevasse due to the subsidence of the
599 SB under its own weight, and (v) perforation in the snow surface due to local collapses of the SB.
600

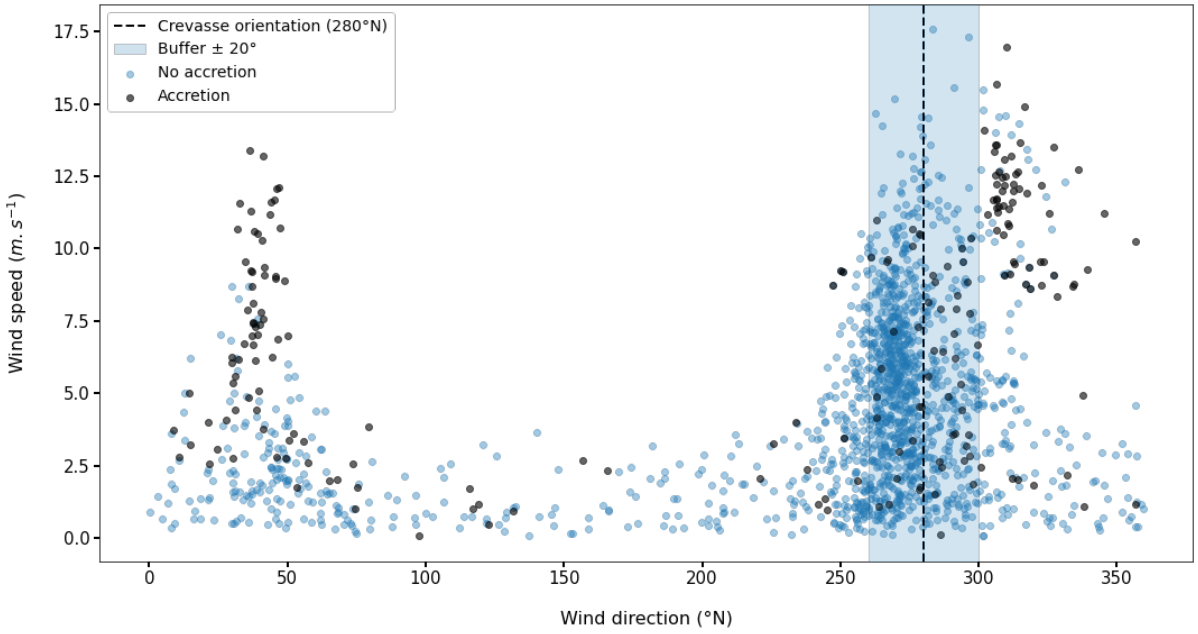


601

602 Fig. 12. Hourly mean wind conditions (speed and direction) from the beginning of the monitoring period (02 Sept. 2016) to
603 the entire overcast of the crevasse by a SB (12 Nov. 2016) with distinction between accretion and non-accretion (possibly
604 WSF) phases.
605

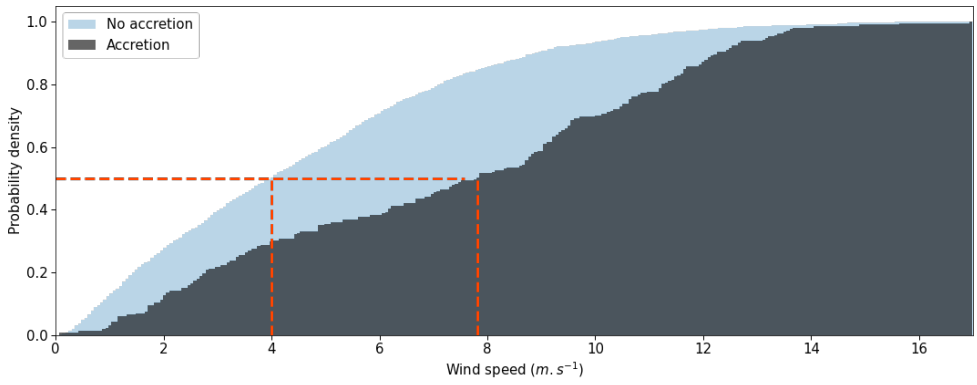


606

Fig. 13. Cumulative probability distribution of respective accretion and non-accretion phases as a function of the mean wind speed for the period 02 Sept. - 12 Nov. 2016.

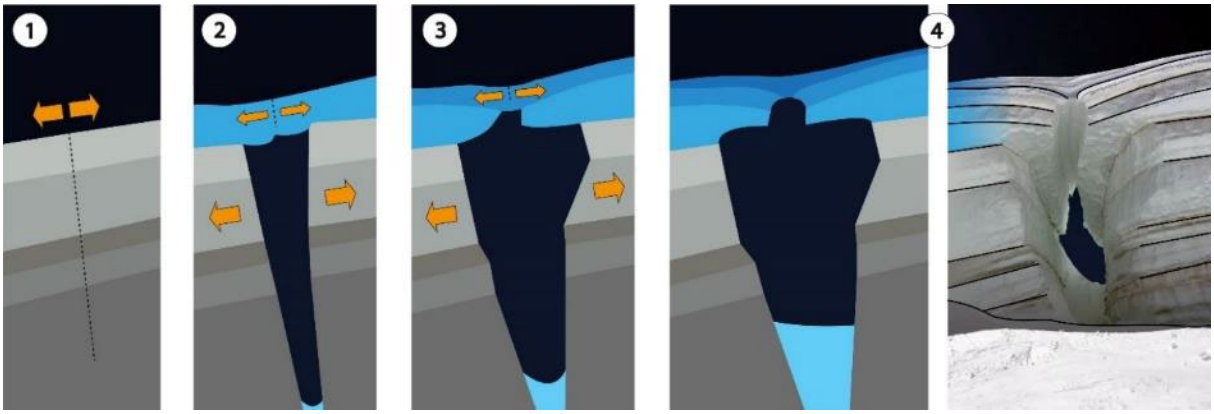


Fig. 14. A type of SB built by successive snow layers as the crevasse opens (*Vallée Blanche*, April 2017; ph. E. Favret).

### 5.2. Weather conditions prone to natural collapses

Ogier et al. (2017) have confirmed the modalities of SBs failure under overload stress initially recognized by Rochelle and Rochelle (2006): local shear failure (perforating failure), total shear failure, and total flexural failure. Here, no failure linked to mountaineers could be observed, the site being off traditional routes. No total failures (*i.e.* across the entire width of the crevasse and over a significant length) were observed during the monitoring period since only 4 local failures occurred. It is likely that total failures only rarely occur in the absence of overloads. They relatively often require an overload by a mountaineer which represents 12 % of the cases documented by Ogier et al. (2017) and mainly concerns large SBs (approximately 1,5-m-thick and 4-m-large on average), generally made of recent snow. With such a failure, important traumatises (sometimes lethal) are caused to practitioners and the rope partner is most of the time pulled down into the crevasse too. As suggested by our data, SBs can mostly degrade 'naturally' by successive local failures.

Figure 15 displays the air temperature conditions for the partial failure of the 12 June 2017. It should be noted that the failure occurred at the level of crevasse **2**, in opening mode at that period, which

favoured the event. The global synoptic situation during the days preceding the failure was a ridge of high pressure, associated with high temperatures (up to 16°C) on the day before the failure and a high flux of solar energy (up to an hourly total of 18.4 MJ/m$^2$). During the two preceding nights, the air temperature stayed largely over 0°C (min.: 5 and 4°C, respectively). These temperatures undoubtedly caused an interruption of the melt-freeze cycles and likely led to high liquid contents in the SB (melting and percolation) with well-rounded and cohesionless particles (Colbeck, 1982; Cagnati et al., 2004). SB has therefore collapsed into the crevasse under its own weight because of a lowered breaking stress threshold (see Vogel et al, 2012, and Hancock et al., 2020, for a cornice falls under positive temperatures in Svalbard). The same situation occurred for the failure of the 20$^{th}$ of June 2017 and, to a lesser extent, for the ones of the 01 May and 18 July 2017. All the partial failures occurred with a likely interruption of the melt-freeze cycles, *i.e.* outside the periods of snow accumulation which are favourable to the breaking of cornices at high latitude (Hancock et al., 2020). As a reminder, 70 % of crevasse accidents recorded by the CNOSM are occurring under a sunny and hot weather.

At the Aiguille du Midi, the mean temperature on the day before the failure of June 2017 was +9.4°C. A situation with an equivalent or higher temperature has only occurred 4 other times between February 2007 and May 2020 (13 years), during two heatwave events (end of June 2017 and end of June 2019). This temperature and the related snow conditions can therefore be considered abnormal. Thus, as the frequency of these hot events increases (*e.g.*, Zampieri et al., 2016), they could be at the origin of more periods of high risk for mountaineers.

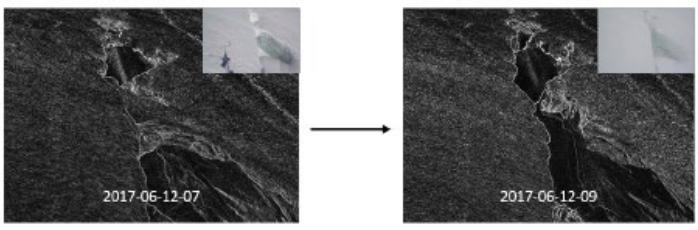

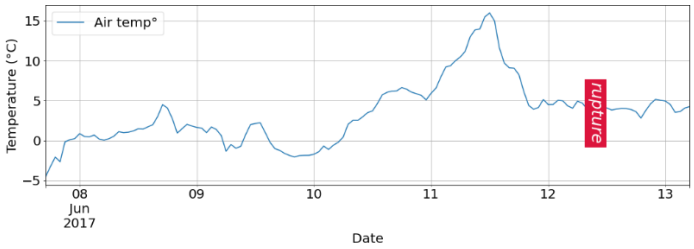


649

650 Fig. 15. Air temperature during the four days preceding the SB failure of the 12 June 2017. Top: images before/after with
651 artificially accentuated edges.

652

653 **5.3. Monitoring difficulties in a highly extreme environment**

654

655 A SB can be extremely variable over a short period of time (possible formation within a few hours to a
656 few days, sudden failure) as well as over a longer-term (progressive formation, evolution over a
657 season). It forms over an object – the glacier – which is also instable and mobile. The differential motion
658 of the glacier caused the tower to move with shroud cables becoming untightened and therefore
659 unable to prevent the tilt of the tower. Moreover, this monitoring was implemented in a climatically
660 extreme and very challenging environment.
661 Despite the fact that we monitored a single site raising the question of its representativeness, the data
662 obtained were sufficient to contribute to the understanding of the formation and evolution of SBs, an
663 object that remain poorly known whilst proper knowledge on its behaviour is necessary to reduce the
664 risk-taking by the high mountain practitioners. One solution could be to monitor various contexts from
665 a topographic and glacier point of view, and to install the monitoring system on a stable support
666 (bedrock). An important limitation would then be the lack of direct measurements at the SB. The local
667 influences are major in such an environment: local topography, wind fields, and large spatial variability
668 of snow cover (*e.g.* Grünewald et al., 2010; Mott and Lehning, 2010). Several other improvements
669 could be added. The use of a heating protection box for the camera could be a determining criterion
670 to increase the number and the image quality. As the SR50A acoustic snow meter did not give
671 satisfactory results and tends to be noisy in windy conditions (*e.g.*, Lv and Pomeroy, 2020), a new

system will be sought. The settlement of multiple temperature sensors in the crevasse could ensure the possibility of working on the metamorphism of the snow constituting the SB together with systematic snow pits within it in order to analyse the snow density and grain properties. Finally, a GSM transmission of the data could help to ensure rapid intervention in case of event/problem associated with the monitoring system.

## 6. Conclusions

A SB is a complex natural object, dangerous for mountaineers, often combining different layers/cornices of snow with different physical properties, themselves modified by the weather conditions, the dynamics of the glacier and the behaviour of the crevasses which can either improve the stability/resistance of the SB (closing crevasse) or lower it (opening).

Despite the extreme conditions met in high mountain environment (high wind, low temperatures) and the difficulties to monitor such a fast-evolving object that a SB can be on a moving glacier, we have succeeded in detailing the evolution of three crevasses and their SBs on one of the tributaries of the Mer de Glace. We have been able to show two main and two secondary cornice accretion events with one creating a complete SB, several periods of wind snow filling of the crevasse including an integral one, and four partial failures.

The main outcomes are the following:

- with a snow cover that does not allow to directly identify crevasses, GPR survey enabled to highlight their presence at the level of bumps formed by the bedrock under a thickness of about 25 m of ice;
- the monitored crevasse pattern has a very low-advection lifecycle, with crevasses opening/closing over a few meters, which is not the most frequent case in glacier accumulation zones;
- a wind event parallel to a crevasse favours its filling by snow, eventually leading to a total filling (no SB and therefore no risk for the practitioner);

- a strong wind making a significant angle with the crevasse can rapidly create a SB by cornice accretion that grows by extending leeward, preferentially under largely negative temperatures;
- on top of these two types of structures, SBs built by successive snow layers deposited as the crevasse opens (low wind) also have to be considered;
- high temperatures and the corresponding melting metamorphism of the snow are responsible for most of the natural failures of SBs, this is all the more evident when there is an interruption of the melt-freeze cycles;
- in the conditions encountered during the study (very little snow accumulation on the glacier), evidences of the presence of a SB – and therefore of a crevasse – are noticeable as long as mountaineers are aware of these field clues: snow surface topography with micro-breaks, snow texture/colour, etc.

We already took advantages of this knowledge to raise the awareness of French (ENSA), Swiss (AVGM) and Italian (UVGAM) mountain guides through training sessions both indoor and in the field. Other activities of popularization are also in progress for the other high mountain practitioners.

**Acknowledgments**

The authors warmly thank M. Fauquet, F. Marsigny, F. Pallandre (ENSA); E. Courcier (*La Chamoniarde*); S. Frendo (*Compagnie des Guides de Chamonix*); G. Guillet (EDYTEM); G. Lesaulnier (CMB), the *Fondazione Montagna Sicura*, as well as *Chamonix Mont Blanc Hélicoptère* and the *Compagnie du Mont Blanc* for their precious help in the field activities. Thanks to C. Jacot (ENSA/CNOSM) for the accident data. The instrumentation was financed by the Interreg V-A France-Italy ALCOTRA project 2014-2020 n°342 *PrévRisk Haute Montagne* with the support of ENSA and EDYTEM-CNRS. The data analysis was supported by a special grant from the *PETZL Foundation* (www.petzl.com/fondation/)

This work is a tribute to A. Revilliod (*La Chamoniarde*) and F. Gentet (ENSA), actors of mountain risk prevention who recently died in mountain.

## References

Arcone, S. A., Lever, J. H., Ray, L. E., Walker, B. S., Hamilton, G., Kaluzienski, L., 2015. Ground-penetrating radar profiles of the McMurdo Shear Zone, Antarctica, acquired with an unmanned rover: Interpretation of crevasses, fractures, and folds within firn and marine ice. Geophysics 81(1): WA21–WA34. https://doi.org/10.1190/geo2015-0132.1

Augros, C., Zanghi, F., 2008. Snow depth measurement at Météo-France. WMO Technical Conference on Instruments and Methods of Observation, St. Petersburg, Russian Federation, 27-29 November 2008. *IOM Report* 9, 8 p. library.wmo.int_Augros

Berthier, E., Vincent, C., 2012. Relative contribution of surface mass-balance and ice-flux changes to the accelerated thinning of Mer de Glace, French Alps, over 1979-2008. *Journal of Glaciology* 58, 501–512. https://doi.org/10.3189/2012JoG11J08

Berthier, E., Vadon, H., Baratoux, D., Arnaud, Y., Vincent, C., Feigl, K.L., Rémy, F., Legrésy, B., 2005. Surface motion of mountain glaciers derived from satellite optical imagery. *Remote Sensing of Environment* 95, 14–28. https://doi.org/10.1016/j.rse.2004.11.005

Berthier, E., Cabot, V., Vincent, C., Six, D., 2016. Decadal region-wide and glacier-wide mass balances derived from multi-temporal ASTER satellite Digital Elevation Models. Validation over the Mont-Blanc area. *Frontiers in Earth Science* 4. https://doi.org/10.3389/feart.2016.00063

Cagnati, A., Crepaz, A., Macelloni, G., Pampaloni, P., Ranzi, R., Tedesco, M., Tomirotti, M., Valt, M., 2004. Study of the snow melt–freeze cycle using multi-sensor data and snow modeling. *Journal of Glaciology* 50(170), 419–426. https://doi.org/10.3189/172756504781830006

747 Chritin, V., Bolognesi, R., Gubler, H., 1999. FlowCapt: A new acoustic sensor to measure snowdrift
748 and wind velocity for avalanche forecasting. *Cold Regions Science and Technology* 30, 125–133.
749 https://doi.org/10.1016/S0165-232X(99)00012-9
750 Colbeck, S.C., 1982. An overview of seasonal snow metamorphism. *Reviews of Geophysics* 20, 45–61.
751 https://doi.org/10.1029/RG020i001p00045
752 Colgan, W., Rajaram, H., Abdalati, W., McCutchan, C., Mottram, R., Moussavi, M.S., Grigsby, S., 2016.
753 Glacier crevasses: Observations, models, and mass balance implications. *Reviews of Geophysics*
754 54, 119–161. https://doi.org/10.1002/2015RG000504
755 Delaney, A.J., Arcone, S.A., O'Bannon, A., Wright, J., 2004. Crevasse detection with GPR across the
756 Ross Ice Shelf, Antarctica. *Proceedings of the Tenth International Conference on Grounds*
757 *Penetrating Radar*, GPR 2004, Delft, Netherlands, pp. 777–780.
758 https://doi.org/10.1109/ICGPR.2004.179867
759 Eckerstorfer, M., Christiansen, H. H., 2011. Topographical and meteorological control on snow
760 avalanching in the Longyearbyen area, central Svalbard 2006–2009. *Geomorphology* 134, 186–
761 196. https://doi.org/10.1016/j.geomorph.2011.07.001
762 Eckerstorfer, M., Christiansen, H.H., Vogel, S., Rubensdotter, L., 2013. Snow cornice dynamics as a
763 control on plateau edge erosion in central Svalbard. *Earth Surface Processes and Landforms* 38,
764 466–476. https://doi.org/10.1002/esp.3292
765 Eder, K., Reidler, C., Mayer, C., Leopold, M., 2008. Crevasse detection in Alpine areas using ground
766 penetrating RaDAR as a component for a mountain guide system. *The International Archives of*
767 *the Photogrammetry, Remote Sensing and Spatial Information Sciences* 37: 837–841.
768 isprs.org_proceedings_XXXVII_congress_WG-VIII-8
769 Fallourd, R., Harant, O., Trouve, E., Nicolas, J., Gay, M., Walpersdorf, A., Mugnier, J.-L., Serafini, J.,
770 Rosu, D., Bombrun, L., Vasile, G., Cotte, N., Vernier, F., Tupin, F., Moreau, L., Bolon, P., 2011.
771 Monitoring temperate glacier displacement by multi-temporal TerraSAR-X images and

772 continuous GPS measurements. *IEEE Journal of Selected Topics in Applied Earth Observations*
773 *and Remote Sensing* 4, 372–386. https://doi.org/10.1109/JSTARS.2010.2096200
774 Fischer, A., Kuhn, M., 2013. Ground-penetrating radar measurements of 64 Austrian glaciers
775 between 1995 and 2010. *Annals of Glaciology* 54, 179–188.
776 https://doi.org/10.3189/2013AoG64A108
777 Gagliardini, O., Meyssonnier, J., 1997. Flow simulation of a firn-covered cold glacier. *Annals of*
778 *Glaciology* 24, 242–248. https://doi.org/10.3189/S0260305500012246
779 Gardent, M., Rabatel, A., Dedieu, J.-P., Deline, P., 2014. Multitemporal glacier inventory of the French
780 Alps from the late 1960s to the late 2000s. *Global and Planetary Change* 120, 24–37.
781 https://doi.org/10.1016/j.gloplacha.2014.05.004
782 Gillet, F., Donnou, D., Ricou, G. 1976. A new electrothermal drill for coring in the ice. In:
783 Splettstoesser, J. F. (ed.) *Ice-core drilling*. University of Nebraska Press, pp. 19–27.
784 Grünewald, T., Schirmer, M., Mott, R., Lehning M., 2010. Spatial and temporal variability of snow
785 depth and ablation rates in as mountain catchment. *The Cryosphere* 4, 215–225.
786 https://doi.org/10.5194/tc-4-215-2010
787 Guillet, G., Preunkert, S., Ravanel, L., Montagnat, M., Friedrich R., 2021. Investigation of a cold-based
788 ice apron on a high-mountain permafrost rock wall using ice texture analysis and micro-$^{14}$C
789 dating: A case study of the Triangle du Tacul ice apron (Mont Blanc massif, France). *Journal of*
790 *Glaciology* 67, 1205–1212. https://doi.org/10.1017/jog.2021.65
791 Hambrey, M.J., Müller, F., 1978. Structures and ice deformation in the White Glacier, Axel Heiberg
792 Island, Northwest Territories, Canada. *Journal of Glaciology* 20, 41–66.
793 https://doi.org/10.3189/S0022143000021213
794 Hancock, H., Eckerstorfer, M., Prokop, A., Hendrikx, J., 2020. Quantifying seasonal cornice dynamics
795 using a terrestrial laser scanner in Svalbard, Norway. *Natural Hazards and Earth System Sciences*
796 20, 603–623. https://doi.org/10.5194/nhess-20-603-2020

797 Harper, J.T., Humphrey, N.F., Pfeffer W.T., 1998. Crevasse patterns and the strain-rate tensor: A high-
798 resolution comparison. *Journal of Glaciology* 44, 68–76.
799 https://doi.org/10.3189/S0022143000002367
800 Herwijnen, A.V., Miller, D.A., 2013. Experimental and numerical investigation of the sintering rate of
801 snow. *Journal of Glaciology* 59, 269–274. https://doi.org/10.3189/2013JoG12J094
802 Heucke, E., 1999. A light portable steam-driven ice drill suitable for drilling holes in ice and firn.
803 *Geografiska Annaler: Series A, Physical Geography* 81, 603–609. https://doi.org/10.1111/1468-
804 0459.00088
805 Holdsworth, G., 1969. Primary transverse crevasses. *Journal of Glaciology* 8, 107–129.
806 https://doi.org/10.3189/S0022143000020797
807 Hopkins, W., 1862. XXXI. On the theory of the motion of glaciers. *Philosophical Transactions of the*
808 *Royal Society of London* 152, 677–745. https://doi.org/10.1098/rstl.1862.0034
809 Jol, H. M., 2009. *Ground Penetrating Radar: Theory and applications*. Elsevier Science, Oxford, UK,
810 544 p. https://doi.org/10.1016/B978-0-444-53348-7.X0001-4
811 Jomelli, V., Delval, C., Grancher, D., Escande, S., Brunstein, D., Hetu, B., Filion, L., Pech, P., 2007.
812 Probabilistic analysis of recent snow avalanche activity and weather in the French Alps. *Cold*
813 *Regions Science and Technology* 47(1-2), 180–192.
814 https://doi.org/10.1016/j.coldregions.2006.08.003
815 Klocker, E., Meuli, L., Rauch, S., Kottmann, A., Mosimann, U., Pasquier, M., Métrailler, P., Doppman,
816 P., Albrecht, R., Pietsch, U., 2022. Crevasse accidents in the Swiss Alps: Epidemiology and
817 mortality of 405 victims of crevasse accidents from 2010 to 2020. *Injury*, 53(1): 183–189.
818 https://doi.org/10.1016/j.injury.2021.08.010
819 Kobayashi, D., Ishikawa, N., Nishio, F., 1988. Formation process and direction distribution of snow
820 cornices. *Cold Regions Science and Technology* 15, 131–136. https://doi.org/10.1016/0165-
821 232X(88)90059-6

822 Latham, J., Montagne, J., 1970. The possible importance of electrical forces in the development of
823 snow cornices. *Journal of Glaciology* 9, 375–384. https://doi.org/10.3189/S0022143000022899
824 Lehning, M., Fierz, C., 2008. Assessment of snow transport in avalanche terrain. *Cold Regions Science*
825 *and Technology* 51(2-3), 240–252. https://doi.org/10.1016/j.coldregions.2007.05.012.
826 Lehning, M., Doorschot, J., Bartelt, P., 2000. A snowdrift index based on SNOWPACK model
827 calculations. *Annals of Glaciology* 31, 382–386. https://doi.org/10.3189/172756400781819770
828 Le Meur, E., Magand, O., Arnaud, L., Fily, M., Frezzotti, M., Cavitte, M., Mulvaney, R., Urbini, S., 2018.
829 Spatial and temporal distributions of surface mass balance between Concordia and Vostok
830 stations, Antarctica, from combined radar and ice core data: first results and detailed error
831 analysis. *The Cryosphere*, 12, 1831–1850. https://doi.org/10.5194/tc-12-1831-2018
832 Li, L., Pomeroy, J.W., 1997. Estimates of threshold wind speeds for snow transport using
833 meteorological data. *Journal of Applied Meteorology and Climatology* 36, 205–213.
834 https://doi.org/10.1175/1520-0450
835 Li, G., Wang, Z. S., Huang, N., 2018. A snow distribution model based on snowfall and snow drifting
836 simulations in mountain area. *Journal of Geophysical Research - Atmosphere* 123(14), 7193–
837 7203. https://doi.org/10.1029/2018JD028434
838 Lv, Z., Pomeroy, J. W., 2020. Assimilating snow observations to snow interception process
839 simulations. *Hydrological processes* 34(10), 2229–2246. https://doi.org/10.1002/hyp.13720
840 Magnin, F., Brenning, A., Bodin X., Deline, P., Ravanel, L., 2015. Statistical modelling of rock wall
841 permafrost distribution: application to the Mont Blanc massif. *Géomorphologie* 21, 145–162.
842 https://doi.org/10.4000/geomorphologie.10965
843 McCarty, D., Brown, R., Montagne, J., 1986. *Cornices: their growth, properties, and control*. *In*:
844 International Snow Science Workshop, Lake Tahoe, pp. 41–45.
845 Marsh, O.J., Price, D., Courville, Z.R., Floricioiu, D., 2021. Crevasse and rift detection in Antarctica
846 from TerraSAR-X satellite imagery. *Cold Regions Science and Technology* 187, 103284.
847 https://doi.org/10.1016/j.coldregions.2021.103284

Möller, T., Tchiguirinskaia, I., Schertzer, D., Dupont, E., Roustan, Y., Bernardara, P., Peinke J., 2018. Multifractal structure of storm Eleanor in France and predictions of the extremes. *Geophysical Research Abstracts* 20, EGU2018-16451-1. EGU2018-16451-1

Mott, R., Lehning, M., 2010. Meteorological modeling of very high-resolution wind fields and snow deposition for mountains. *Journal of Hydrometeorology* 11, 934–949. https://doi.org/10.1175/2010JHM1216.1

Mott, R., Schirmer, M., Bavay, M., Grünewald, T., Lehning, M., 2010. Understanding snow-transport processes shaping the mountain snow-cover. *The Cryosphere* 4, 545–559. https://doi.org/10.5194/tc-4-545-2010

Mourey, J., Marcuzzi, M., Ravanel, L., Pallandre, F., 2019. Effects of climate change on high Alpine mountain environments: Evolution of mountaineering routes in the Mont Blanc massif (Western Alps) over half a century. *Arctic, Antarctic, and Alpine Research* 51, 176–189. https://doi.org/10.1080/15230430.2019.1612216

Munroe, J.S., 2018. Monitoring snowbank processes and cornice fall avalanches with time-lapse photography. *Cold Regions Science and Technology* 154, 32–41. https://doi.org/10.1016/j.coldregions.2018.06.006

Naaim-Bouvet, F., Guyomarc'h, G., Naaim, M., Durand, Y., Bellot, H., Pugliese, P., 2012. Transport de neige par le vent sur un site de haute montagne : de la modélisation à l'observation, de l'observation à la modélisation. *La Houille Blanche* 98, 51–57. https://doi.org/10.1051/lhb/2012008

Nath, P.C., Vaughan, D.G., 2003. Subsurface crevasse formation in glaciers and ice sheets. *Journal of Geophysical Research: Solid Earth* 108, 7–12. https://doi.org/10.1029/2001JB000453

Ogier, C., Ravanel, L., Graff, E., 2017. Parcours glaciaires et rupture de ponts de neige – Premières connaissances issues de retours d'expérience. *Neige et Avalanches* 158, 18–21. hal-01779608

872 Pasquier, M., Taffé, P., Kottmann, A., Mosimann, U., Reisten, O., Hugli, O., 2014. Epidemiology and
873 mortality of glacier crevasse accidents. *Injury* 45, 1700–1703.
874 https://doi.org/10.1016/j.injury.2014.07.001
875 Pomeroy, J.W., Gray, D.M., 1990. Saltation of snow. *Water Resources Research* 26, 1583–1594.
876 https://doi.org/10.1029/WR026i007p01583
877 Pralong, A., Funk, M., 2005. Dynamic damage model of crevasse opening and application to glacier
878 calving. *Journal of Geophysical Research: Solid Earth* 110.
879 https://doi.org/10.1029/2004JB003104
880 Prokop, A., Procter, E.S., 2016. A new methodology for planning snow drift fences in Alpine terrain.
881 *Cold Regions Science and Technology* 132, 33–43.
882 https://doi.org/10.1016/j.coldregions.2016.09.010
883 Rabatel, A., Letréguilly, A., Dedieu, J.-P., Eckert, N., 2013. Changes in glacier equilibrium-line altitude
884 in the western Alps from 1984 to 2010: Evaluation by remote sensing and modeling of the
885 morpho-topographic and climate controls. *The Cryosphere* 7, 1455–1471.
886 https://doi.org/10.5194/tc-7-1455-2013
887 Réveillet, M., Vincent, C., Six, D., Rabatel, A., Sanchez, O., Piard, L., Laarman, O., 2021. Spatio-
888 temporal variability of surface mass balance in the accumulation zone of the Mer de Glace,
889 French Alps, from multitemporal terrestrial LiDAR measurements. *Journal of Glaciology* 67, 137–
890 146. https://doi.org/10.1017/jog.2020.92
891 Rochelle, R.R., Rochelle, R.D., 2006. Glacier snow bridge mechanics. *In*: *Proceedings of the 2006*
892 *International Snow Science Workshop (ISSW), Telluride*, pp. 193–202. arc.lib.montana.edu-issw-
893 2006-193-202
894 Salim, E., Mourey, J., Ravanel, L., Picco, P., Gauchon, C., 2019. Mountain guides facing the effects of
895 climate change. What perceptions and adaptation strategies at the foot of Mont Blanc? *Journal*
896 *of Alpine Research* 107, 5865, 14 p. https://doi.org/10.4000/rga.5865
897 Sandmeier, K., 2004. *ReflexW manual ver. 3.5*. Karlsruhe Sandmeier Scientific Software. 377 pp.

898 Schneider, C.A., Rasband, W.S., Eliceiri, K.W., 2012. NIH Image to ImageJ: 25 years of image analysis.
899 *Nature Methods* 9, 671–675. https://doi.org/10.1038/nmeth.2089
900 Schmidt, R., 1980. Threshold wind-speeds and elastic impact in snow transport. *Journal of Glaciology*
901 26(94), 453–467. https://doi.org/10.3189/S0022143000010972
902 Schweizer, J., Jamieson, J. B., Schneebeli, M., 2003. Snow avalanche formation. *Reviews of*
903 *Geophysics* 41(4). https://doi.org/10.1029/2002RG000123
904 Seity, Y., Brousseau, P., Malardel, S., Hello, G., Bénard, P., Bouttier, F., Lac, C., Masson, V., 2011. The
905 AROME-France Convective-Scale Operational Model. *Monthly Weather Review* 139, 976–991.
906 https://doi.org/10.1175/2010MWR3425.1
907 Singh, K.K., Negi, H.S., Ganju, A., Kulkarni, A.V., Kumar, A., Mishra, V.D., Kumar, S., 2013. Crevasses
908 detection in Himalayan glaciers using ground-penetrating radar. *Current Science* 105, 1288–
909 1295. https://www.jstor.org/stable/24098940
910 Six D., Vincent, C., 2014. Sensitivity of mass balance and equilibrium-line altitude to climate change in
911 the French Alps. *Journal of Glaciology* 60, 867–878. https://doi.org/10.3189/2014JoG14J014
912 Smith, R.A., 1976. The application of fracture mechanics to the problem of crevasse penetration.
913 *Journal of Glaciology* 17, 223–228. https://doi.org/10.3189/S0022143000013563
914 Sokratov, S.A., Sato, A., 2001. The effect of wind on the snow cover. *Annals of Glaciology* 32, 116–
915 120. https://doi.org/10.3189/172756401781819436
916 Teufelsbauer, H., 2011. A two-dimensional snow creep model for alpine terrain. *Natural Hazards* 56,
917 481–497. https://doi.org/10.1007/s11069-010-9515-8
918 Trouvé, E., Vasile, G., Gay, M., Bombrun, L., Grussenmeyer, P., Landes, T., Nicolas, J.-M., Bolon, P.,
919 Petillot, Y., Julea, A., Valet, L., Chanussot, J., Koehl, M., 2007. Combining airborne photographs
920 and spaceborne SAR data to monitor temperate glaciers: potentials and limits. *IEEE Transactions*
921 *on Geoscience and Remote Sensing* 45, 905–924. https://doi.org/10.1109/TGRS.2006.890554

van der Veen, C.J., 1998. Fracture mechanics approach to penetration of surface crevasses on glaciers. *Cold Regions Science and Technology* 27, 31–47. https://doi.org/10.1016/S0165-232X(97)00022-0

van der Veen, C.J., 1999. Crevasses on glaciers. *Polar Geography* 23, 213–245. https://doi.org/10.1080/10889379909377677

Vaughan, D.G., 1993. Relating the occurrence of crevasses to surface strain rates. *Journal of Glaciology* 39, 255–266. https://doi.org/10.3189/S0022143000015926

Veilleux, S., Decaulne, A., Bhiry, N., 2021. Snow cornice and snow avalanche monitoring using automatic time lapse cameras in Tasiapik Valley, Nunavik (Québec) during the winter of 2017–2018. *Arctic Science* 7, 798–812. https://doi.org/10.1139/as-2020-0013

Vincent, C., Vallon, M., Pinglot, J.-F., Funk, M., Reynaud, L., 1997. Snow accumulation and ice flow at Dôme du Goûter (4300 m), Mont Blanc, French Alps. *Journal of Glaciology* 43, 513–21. https://doi.org/10.3189/S0022143000035127

Vincent, C., Soruco, A., Six, D., Le Meur, E., 2009. Glacier thickening and decay analysis from 50 years of glaciological observations performed on Glacier d'Argentière, Mont Blanc area, France. *Annals of Glaciology* 50, 73–79. https://doi.org/10.3189/172756409787769500

Vogel, S., Eckerstorfer, M., Christiansen, H.H., 2012. Cornice dynamics and meteorological control at Gruvefjellet, Central Svalbard. *The Cryosphere* 6, 157–171. https://doi.org/10.5194/tc-6-157-2012

Vornberger, P.L., Whillans, I.M., 1990. Crevasse deformation and examples from Ice Stream B, Antarctica. *Journal of Glaciology* 36, 3–10. https://doi.org/10.3189/S0022143000005487

Wever, N., Vera Valero, C., Fierz, C., 2016. Assessing wet snow avalanche activity using detailed physics based snowpack simulations. *Geophysical Research Letters* 43, 5732–5740. https://doi.org/10.1002/2016GL068428

946 Wiese, M., Schneebeli, M., 2017. Early-stage interaction between settlement and temperature-
947 gradient metamorphism. *Journal of Glaciology* 63, 652–662.
948 https://doi.org/10.1017/jog.2017.31
949 Woodward, J., Burke, M.J., 2007. Applications of Ground-Penetrating Radar to glacial and frozen
950 materials. *Journal of Environmental and Engineering Geophysics* 12, 69–85.
951 https://doi.org/10.2113/JEEG12.1.69
952 Xie, Z., Ma, Y., Ma, W., Hu, Z., Sun, G., 2021. The statistics of blowing snow occurrences from multi-
953 year autonomous snow flux measurements in the French Alps. *The Cryosphere Discussions*, 1–
954 23. https://doi.org/10.5194/tc-2021-260
955 Yang, L., Guo, H., Yang, S., Hoshino, Y., Suzuki, S., Gao, D., Cao, Y., 2019. Generation of a high-
956 precision Digital Elevation Model for fields in mountain regions using RTK-GPS. *International*
957 *Journal of Automation Technology* 13, 671–678. https://doi.org/10.20965/ijat.2019.p0671
958 Yu, H., Li, G., Walter, B., Lehning, M., Zhang, J., Huang, N., 2022. Environmental conditions for snow
959 cornice formation tested in a wind tunnel. *The Cryosphere Discuss.* [preprint], in review.
960 https://doi.org/10.5194/tc-2022-27
961 Zamora, R., Casassa, G., Rivera, A., Ordenes, F., Neira, G., Araya, L., Mella, R., Bunster, C., 2007.
962 Crevasse detection in glaciers of southern Chile and Antarctica by means of Ground Penetrating
963 Radar. *In*: Selected papers of the IAHS Assembly in Foz do Iguaçu, Brazil, 2005. *IASH publ.* 318, 10
964 p. academia.edu-Crevasse_detection
965 Zampieri, M., Russo, S., di Sabatino, S., Michetti, M., Scoccimarro, E., Gualdi, S., 2016. Global
966 assessment of heat wave magnitudes from 1901 to 2010 and implications for the river discharge
967 of the Alps. *Science of The Total Environment* 571, 1330–61339.
968 https://doi.org/10.1016/j.scitotenv.2016.07.008